SANDIA REPORT

SAND2018-10958
Unlimited Release
Printed September, 2018

Characterization of a Silicon photo-multiplier summing breakout board for photo-multiplier tube replacement

Team Members: Melinda Sweany, Peter Marleau,
Gene Kallenbach

Prepared by
Sandia National Laboratories
Albuquerque, New Mexico 87185 and Livermore, California 94550

Sandia National Laboratories is a multimission laboratory managed and operated by National Technology and Engineering Solutions of Sandia, LLC., a wholly owned subsidiary of Honeywell International, Inc., for the U.S. Department of Energy's National Nuclear Security Administration under contract DE-NA0003525.

Sandia National Laboratories

Issued by Sandia National Laboratories, operated for the United States Department of Energy by Sandia Corporation.

Available to DOE and DOE contractors from
U.S. Department of Energy
Office of Scientific and Technical Information
P.O. Box 62
Oak Ridge, TN 37831

Telephone: (865) 576-8401
Facsimile: (865) 576-5728
E-Mail: reports@adonis.osti.gov
Online ordering: http://www.osti.gov/bridge

Available to the public from
U.S. Department of Commerce
National Technical Information Service
5285 Port Royal Rd
Springfield, VA 22161

Telephone: (800) 553-6847
Facsimile: (703) 605-6900
E-Mail: orders@ntis.fedworld.gov
Online ordering: http://www.ntis.gov/help/ordermethods.asp?loc=7-4-0#online

SAND2018-10958
Unlimited Release
Printed September, 2018

Characterization of a Silicon photo-multiplier summing breakout board for photo-multiplier tube replacement

Melinda D. Sweany Peter A. Marleau Gene A. Kallenbach

Abstract

We present the relative timing and pulse-shape discrimination performance of a H1949-50 photomultiplier tube to SensL ArrayX-BOB6_64S coupled to a SensL ArrayC-60035-64P-PCB Silicon Photomultiplier array. The goal of this work is to enable the replacement of photomultiplier readout of scintillators with Silicon Photomultiplier devices, which are more robust and have higher particle detection efficiency. The report quantifies the degradation of these performance parameters using commercial off the shelf summing circuits, and motivates the development of an improved summing circuit: the pulse-shape descrimination figure-of-merit drops from 1.7 at 500 keVee to 1.4, and the timing resolution (σ) is 288 ps for the photomultiplier readout and approximately 1 ns for the Silicon Photomultiplier readout. A degradation of this size will have a large negative impact on any device that relies on timing coincidence or pulse-shape discrimination to detect neutron interactions, such as neutron kinematic imaging or multiplicity measurements.

Acknowledgment

Sandia National Laboratories is a multimission laboratory managed and operated by National Technology and Engineering Solutions of Sandia, LLC, a wholly owned subsidiary of Honeywell International, Inc., for the U.S. Department of Energy's National Nuclear Security Administration under contract DE-NA0003525.

We would like to thank the US DOE National Nuclear Security Administration, Office of Defense Nuclear Non-proliferation for funding this work.

The team would like to thank our collaborators at AWE, notably Chris Allwork and Mark Ellis, for helpful guidance involving this work. Steven Hammon performed the circuit layout for the SNL developed summing board.

Contents

1 Introduction **9**

Effective Area 10

Readout Electronics and Data Acquisition 10

2 Photomultiplier tube response **13**

Energy Response 14

Timing Response 14

Particle Identification 15

3 SensL ArrayX-BOB6_64S Summing Board **17**

Energy Response 20

Particle Identification 20

Timing Response 21

4 SNL's summing board **25**

5 Discussion and Conclusion **29**

Appendix

A **33**

A.1 SiPM replacement for PMT Objectives 33

A.2 Design Derivation 34

A.3 SensL Fast Output 35

A.4 Block Diagram 38
A.5 Schematics, Layout and Photos 39
A.6 Testing 39
A.7 Conclusion 45

B **47**

References **58**

List of Figures

1.1 The emission spectrum of stilbene (black) overlaid with the photo-detection efficiency of a C-series SiPM (red) and H1949-50 PMT (blue). 11

2.1 The geometry setup of the timing calibration. The test PMT and stilbene crystal are placed opposite PMT A and PMT B, both also coupled with optical grease to a 2 inch stilbene crystal. The test PMT and PMTs A and B are separated by 10 inches (face-to-face) with a ^{22}Na source placed between them, and PMT A and PMT B are 2.5 inches apart (center-to-center) 13

2.2 The calibrated energy spectrum acquired with a ^{22}Na source for all three H1949 PMTs in the configuration shown in Figure 2.1. The test PMT is shown in black, and PMTs A and B are shown in red and blue, respectively. . 14

2.3 The time difference between (a) H1949-50 "Test" compared to H1949-50 A, (b) H1949-50 "Test" compared to H1949-50 B, and (c) A-B. 15

2.4 The pulse-shape discrimination calibration for (a) H1949-50 test PMT (b) H1949-50 A PMT and (c) H1949-50 B PMT. 16

3.1 The 2" stilbene crystal coupled to SensL's 8x8 array of C-series 6x6 mm SiPMs, and readout by SensL's ArrayX-BOB6_64S summing board. SensL's recommended setup. In order to readout the summed SOUT signal, a capacitor and resistor are connected to jumper pins with the provided by the jumper wires. 17

3.2 Example waveforms from the SensL summing board readout with (a) noise on a scintillation pulse that is not filtered by our signal processing (b) a trigger on noise only, and (c) noise on a scintillation pulse that is filtered out by our signal processing. 18

3.3 The same waveform in Figure 3.2, (a) with the filter parameters used in the analysis and (b) a greater filter width for improved noise reduction. Although increasing the filter width does remove the noise, the timing response is reduced. Offline single processing cannot improve the data acquisition threshold. 18

3.4 The experimental setup with SensL's summing board shielded with a mu-metal box. The box is 5 sided: the lid is not shown here. 19

3.5 Example waveforms with the SensL board readout in the shielded configuration. There is still a source of low-frequency noise (a), however the rate is low enough to push the trigger threshold down. The high frequency noise observed previously is absent (b). 19

3.6 The energy spectrum from the SensL readout from a Na-22 source in the shielded (red) and unshielded (red) configurations. The high trigger threshold necessary to obtain a reasonable event rate due to electronic noise in the unshielded configuration is visible at approximately 200 keVee. 20

3.7 (a) The pulse-shape discrimination calibration for the SensL array in the unshielded configuration. (b) The PSD parameter as a function of energy for SensL's summing board in the shielded configuration. 21

3.8 The time difference between (a) the SensL summing board readout compared to H1949-50 A and (b) the SensL summing board readout compared to H1949-50 B. 22

3.9 The time difference between (a) the shielded SensL summing board readout compared to H1949-50 A and (b) compared to H1949-50 B. 23

4.1 Example waveforms from SNL's summing board readout: (a) a saturated pulse (b) a nominal waveform (c) effect not fully understood. All waveforms have a ∼500 MHz noise that is filtered out during signal processing (the red curves are post-filtering). 26

4.2 The energy spectrum from a ^{22}Na source readout with the SNL summing board 26

4.3 The pulse-shape discrimination readout with the SNL summing board from a (a) ^{22}Na source and (b) AmBe source. The calibrated PSD response with the mean and standard deviation for the neutron and gamma bands is shown in (c), with the neutron trends in red and the gamma response in black. 27

5.1 A comparison between the PMT readout and SiPM readout of a 2" stilbene crystal 30

5.2 A comparison of the PSD response from the PMT readout (a) and SiPM readout (b). 30

5.3 A comparison of the timing response from the PMT readout (a) and SiPM readout (b). 31

Chapter 1

Introduction

One of the most ubiquitous radiation detector systems consists of a photomultiplier tube (PMT) coupled to a scintillating material, such as liquid or plastic organic scintillator, or one of many scintillating inorganic crystals. While widely used for a variety of applications, the size and robustness of such a system is fundamentally limited by the size and robustness of PMTs. One alternative is micro-channel plate PMTs (MCP-PMTs), which are smaller and more robust to magnetic fields. However, they still require high voltage operation (typically above 1kV), require a vacuum tube, and are much more expensive than traditional PMTs: they are more suited to applications which require excellent timing response on the order of 10s of ps. Recently, silicon photo-multipliers (SiPMs) have demonstrated the necessary gain and dark current levels for single photon detection, potentially allowing it to replace PMTs in many applications. The timing response has been demonstrated to be sufficient for particle identification via pulse-shape discrimination [1, 4, 3]. The price of current devices is also competitive with traditional PMTs of similar photo-cathode coverage. SiPMs have other features that improve the robustness and useability compared to traditional PMTS: they are compact, operate on low voltage (typically under 100V), and, like MCP-PMTs, they are insensitive to magnetic fields. Finally, the photo-detection efficiency is much less dependent on the incident position or angle of the photon compared to PMTs: typical PMT responses at 60° incidence drops to approximately 60% of the value at zero incidence [5], while recent measurements on SiPMs report a constant response as a function of incidence angle out to approximately 65° [6]. However, commercial SiPMs are only found in sizes up to 6x6mm^2. In order to cover larger areas (typically several square inches in scintillation detectors), many SiPMs will have to be summed. Summing may adversely affect the overall performance with respect to timing, PSD capability, and overall noise.

In this work, we report on the development of a SiPM-based readout of a 2" stilbene crystal, and compare to a PMT-based readout. We use the 8x8 array of 6x6 mm^2 C-series SiPMs from SensL (ArrayC-60035-64P-PCB). In order to realize the complete replacement of PMT assemblies with SiPMs, it is necessary to develop a compact printed circuit board (PCB) that mates to an array of SiPMs, and sums the individual response of each SiPM in the array. While SensL provides a PCB that mates to their ArrayC-60035-64P-PCB (ArrayX-BOB6_64S), it is nearly twice the cross section of the SiPM array, making it an impractical solution for anything but a bench-top demonstrator.

We therefore developed of a summing board to improve on commercial summing board

for applications that benefit from increasingly accurate pulse shape and timing. As a baseline, we compare the SensL summing board coupled to a 2 inch cylindrical stilbene crystal to a Hamamatsu 1949-50 PMT coupled to the same crystal. Below we characterize the timing response, energy response, and pulse shape discrimination of both the photodetector readouts.

Effective Area

Compared to the PMT readout, the SiPM-based readout differs in photo-detection efficiency (ϵ_{PD}) and photo-detector area (A_{PD}). We characterize the total number of detectable photons as the effective area, defined as

$$A_{eff} = A_{PD} \int N_p(\lambda)\epsilon_{PD}(\lambda)d\lambda, \tag{1.1}$$

in which the number of emitted scintillation photons, N_λ, must pass a wavelength dependent quantum efficiency cut that is characteristic of the photodetector. This does not take into account effects such as the reflectivity on the face of the photo-detector compared to SiPMs, or the angular dependence of the quantum/particle-detection efficiency. Although those effects may be significant, what we hope to provide is a first order adjustment of the relative detection efficiency between the two readout schemes. Here we use the emission spectrum of Stilbene as an example: Figure 1.1 shows the wavelength-dependent output of Stilbene along with the photo-detection efficiencies of the C-series SiPM and H1949-50 PMT. At 1 MeV, stilbene has a yield of 13000 photons, 4306 of which are detectable after applying the wavelength dependent quantum efficiency of the photo-detector and 4805 of which are detectable after applying the photo-detection efficiency of the C-series SiPMs. In terms of photocathode area, the SiPM readout and PMT readout cover the same portion of the stilbene crystal, however the fill factor of the SiPM board is 83.3% caused by gaps between the SiPMs. Therefore, the PMT-based readout has an effective area 1.08% of the SiPMs effective area. This factor will be used to compare the relative detection efficiency between the two detector assemblies.

Readout Electronics and Data Acquisition

All measurements are acquired with a CAEN DT5730 14-bit 500 MS/s digitizer with DPP_PSD firmware. We acquire full waveforms on all channels with any one channel in the setup passing a threshold. However, because the polarity differs between the SiPM and PMT readout and the polarity of the entire digitizer is set, we are effectively acquiring all channels on only one polarity readout over threshold. The effects of this detail are considered to be minor and are described in detail for each measurement below. The waveforms are saved in a ROOT data tree format [7] for further analysis utilizing the ROOT toolkit.

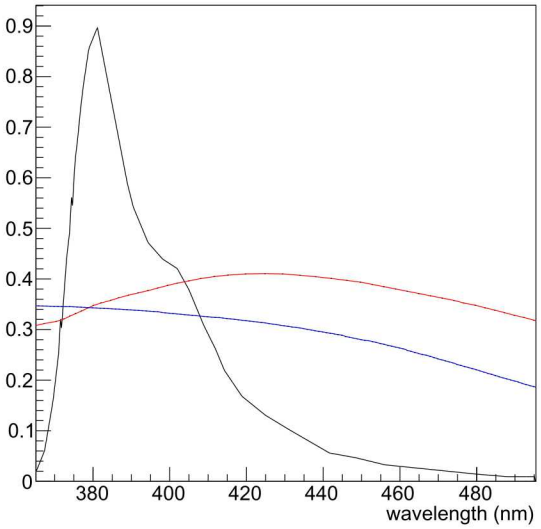

Figure 1.1: The emission spectrum of stilbene (black) overlaid with the photo-detection efficiency of a C-series SiPM (red) and H1949-50 PMT (blue).

Chapter 2

Photomultiplier tube response

We acquired six different datasets to characterize the baseline response from a 2 inch Hamamatsu 1949-50 PMT coupled to a 2" stilbene crystal wrapped in teflon. Figures 2.1 show the measurement configurations for the six datasets. The energy response of the PMT readout is characterized with ^{22}Na. The timing response is characterized with the coincident back-to-back 511 keV gamma emissions from the positron beta decay of a ^{22}Na source. Finally, an AmBe measurement is performed to evaluate the pulse-shape discrimination.

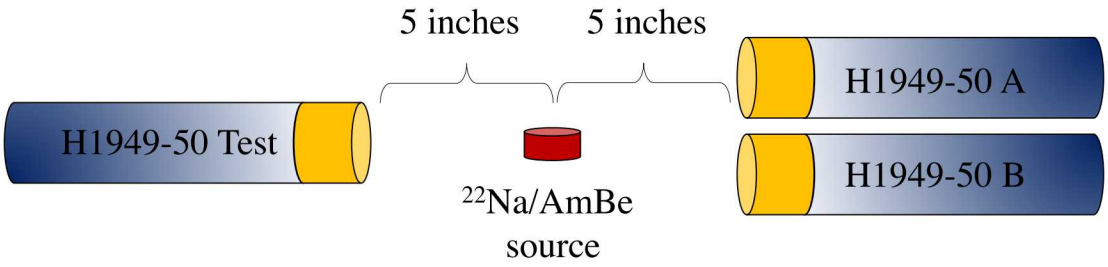

Figure 2.1: The geometry setup of the timing calibration. The test PMT and stilbene crystal are placed opposite PMT A and PMT B, both also coupled with optical grease to a 2 inch stilbene crystal. The test PMT and PMTs A and B are separated by 10 inches (face-to-face) with a ^{22}Na source placed between them, and PMT A and PMT B are 2.5 inches apart (center-to-center)

Energy Response

Figure 2.2 shows the calibrated energy spectrum acquired with a ^{22}Na source for all three H1949 PMTs in the configuration shown in Figure 2.1. The energy resolution for all three PMTs is comparable. The gain of the test tube is slightly lower, as indicated by the higher trigger threshold at 50 keVee compared to approximately 20 keVee for PMTs A and B.

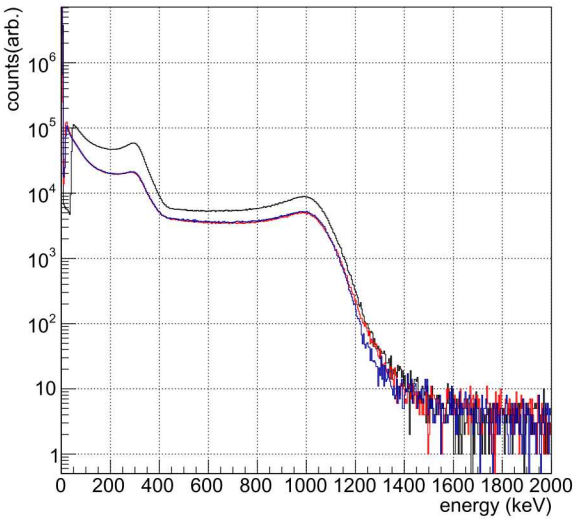

Figure 2.2: The calibrated energy spectrum acquired with a ^{22}Na source for all three H1949 PMTs in the configuration shown in Figure 2.1. The test PMT is shown in black, and PMTs A and B are shown in red and blue, respectively.

Timing Response

The timing response is shown in Figure 2.3: the time difference between interactions in the test PMT and each of the A and B PMTs is shown, with the requirement that the deposited energy in both PMTs is below 500 keVee. Assuming the resolutions are independent, the standard deviation of each distribution in Figure 2.3 is

$$\sigma_{T-A}^2 = \sigma_T^2 + \sigma_A^2 \quad (2.1)$$
$$\sigma_{T-B}^2 = \sigma_T^2 + \sigma_B^2 \quad (2.2)$$
$$\sigma_{A-B}^2 = \sigma_A^2 + \sigma_B^2. \quad (2.3)$$

Solving for σ_T gives a timing resolution of 288 ps for the test PMT:

$$\sigma_T = \sqrt{\frac{\sigma_{A-T}^2 + \sigma_{B-T}^2 - \sigma_{A-B}^2}{2}} = 288 \text{ ps}. \tag{2.4}$$

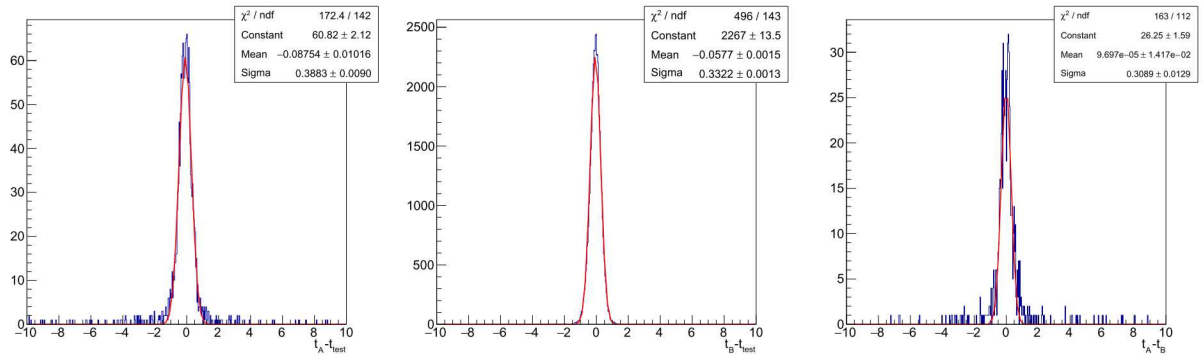

(a) (b) (c)

Figure 2.3: The time difference between (a) H1949-50 "Test" compared to H1949-50 A, (b) H1949-50 "Test" compared to H1949-50 B, and (c) A-B.

Particle Identification

The pulse-shape parameter used in this work is defined as the time it takes for the pulse to develop 75% of its total integral from a pulse start time (taken to be the time at 10% of the pulse's total integral). It was found that using 75% of the total integral maximized the gamma-ray/neutron discrimination, quantified by the figure-of-merit at 2000 keVee. The figure-of-merit is defined as

$$FoM = \frac{\mu_n - \mu_\gamma}{2.355(\sigma_n + \sigma_\gamma)}, \tag{2.5}$$

where $\mu_{n/\gamma}$ is the mean of a Gaussian fit to the neutron and gamma distributions, $\sigma_{n/\gamma}$ is the standard deviation of the Gaussian fit, and the factor of 2.355 is for conversion to a FWHM width. The FoM at 2000 keVee is 2.9 for PMT A and 3.0 for PMT B. At 500 keVee, this drops to 1.7 for both PMTs.

The calibrated PSD parameter as a function of energy for all PMTs is shown in Figure 2.4: the mean of the gamma and neutron populations are indicated by solid lines (red for neutrons and black for gammas), and the upper and lower bounds are indicated by dashed lines (red for neutrons and black for gammas).

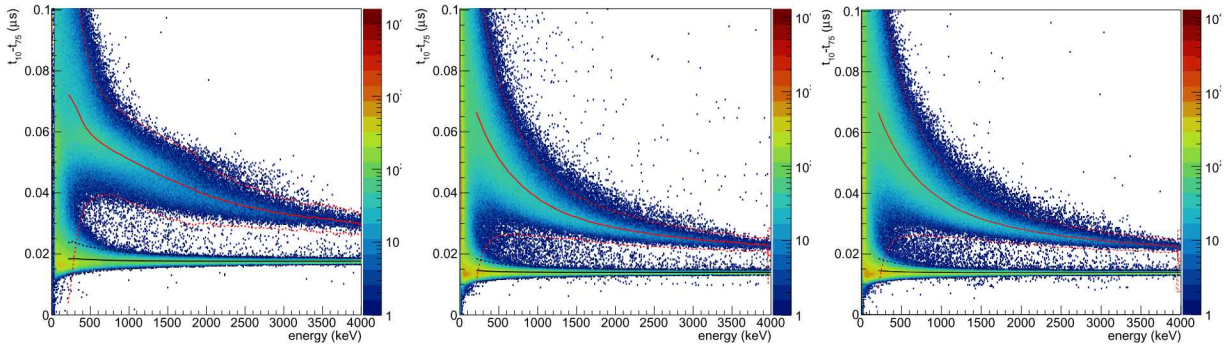

(a) (b) (c)

Figure 2.4: The pulse-shape discrimination calibration for (a) H1949-50 test PMT (b) H1949-50 A PMT and (c) H1949-50 B PMT.

Chapter 3

SensL ArrayX-BOB6_64S Summing Board

The same 2" right cylinder of Stilbene from Inrad Optics was coupled to SensL's ArrayC 6x6mm array, which was mated to SensL's summing board. As recommended by the manufacturer, the summing board was configured for negative bias and readout on the output through a 10 nF coupling capacitor. Figure 3.1 shows the Stilbene crystal coupled to the SiPM array and summing board, and the jumper wires necessary to readout the summing board. All measurements were performed at a bias of (-)29.5 V, provided by a BK Precision DC power supply. We found that the bias voltage could drift by as much as 0.02 V throughout the measurements, which were periodically corrected for by hand.

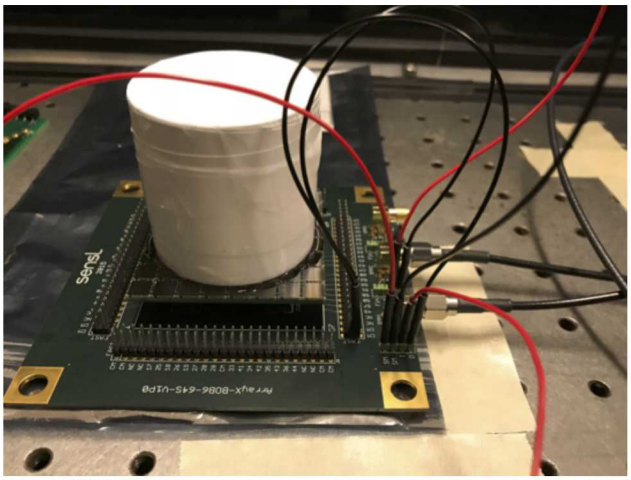

Figure 3.1: The 2" stilbene crystal coupled to SensL's 8x8 array of C-series 6x6 mm SiPMs, and readout by SensL's ArrayX-BOB6_64S summing board. SensL's recommended setup. In order to readout the summed SOUT signal, a capacitor and resistor are connected to jumper pins with the provided by the jumper wires.

This configuration resulted in a lot of noise pickup due to the 5" long jumper wires provided by SensL to used to connect the jumper bins. This caused problems with data acquisition rates and in subsequent signal processing. Periodically the noise rates exceeded the digitizer's ability to acquire data, requiring that the trigger threshold be raised. Our signal processing includes a low-pass filter, which has some success at removing this noise

from scintillator pulses, however some noise remains. Increasing the smoothing of the filter, as demonstrated in Figure 3.3, reduces noise, but has a negative impact on the timing response. Offline signal processing does not improve the data acquisition threshold.

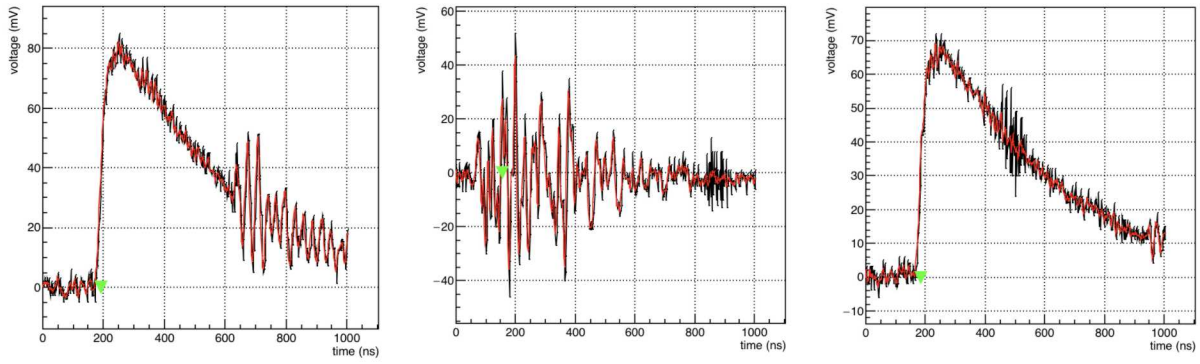

(a) (b) (c)

Figure 3.2: Example waveforms from the SensL summing board readout with (a) noise on a scintillation pulse that is not filtered by our signal processing (b) a trigger on noise only, and (c) noise on a scintillation pulse that is filtered out by our signal processing.

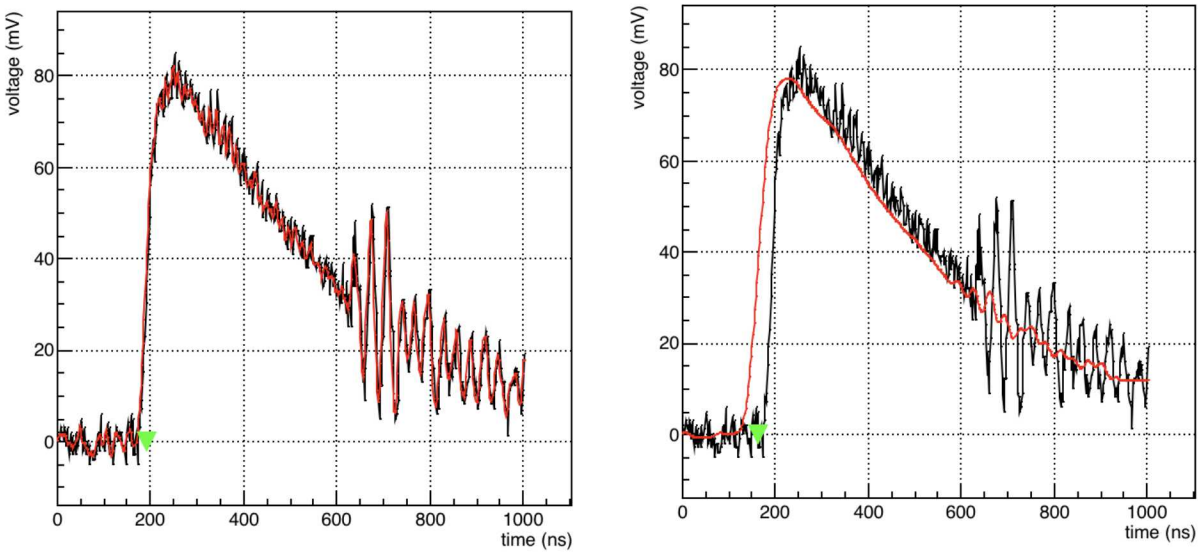

(a) (b)

Figure 3.3: The same waveform in Figure 3.2, (a) with the filter parameters used in the analysis and (b) a greater filter width for improved noise reduction. Although increasing the filter width does remove the noise, the timing response is reduced. Offline single processing cannot improve the data acquisition threshold.

In order to address these noise issues, ^{22}Na and AmBe data were acquired with the summing board inside a mu-metal box for shielding. Figure 3.4 shows the experimental setup: the box is 5-sided with no bottom and a removable top, not shown in the figure but deployed for the measurements. This configuration did reduce the high frequency noise

issues, but an additional lower frequency noise is still present in the data. Figure 3.5a shows this low-frequency noise, and Figure 3.5b shows a representative pulse from the shielded data, with the high-frequency noise absent. This low-frequency noise is unlikely to pass our software pulse threshold.

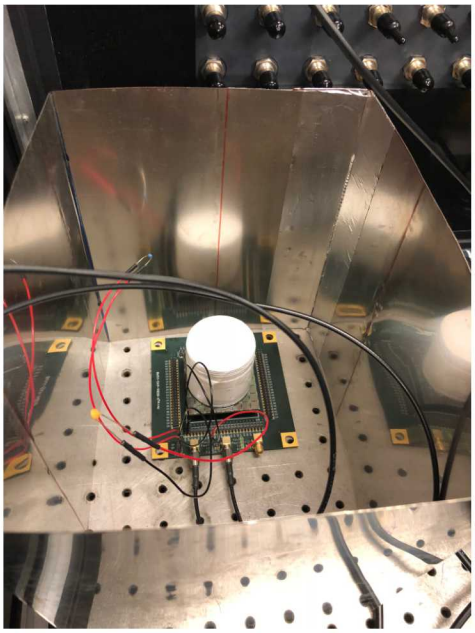

Figure 3.4: The experimental setup with SensL's summing board shielded with a mu-metal box. The box is 5 sided: the lid is not shown here.

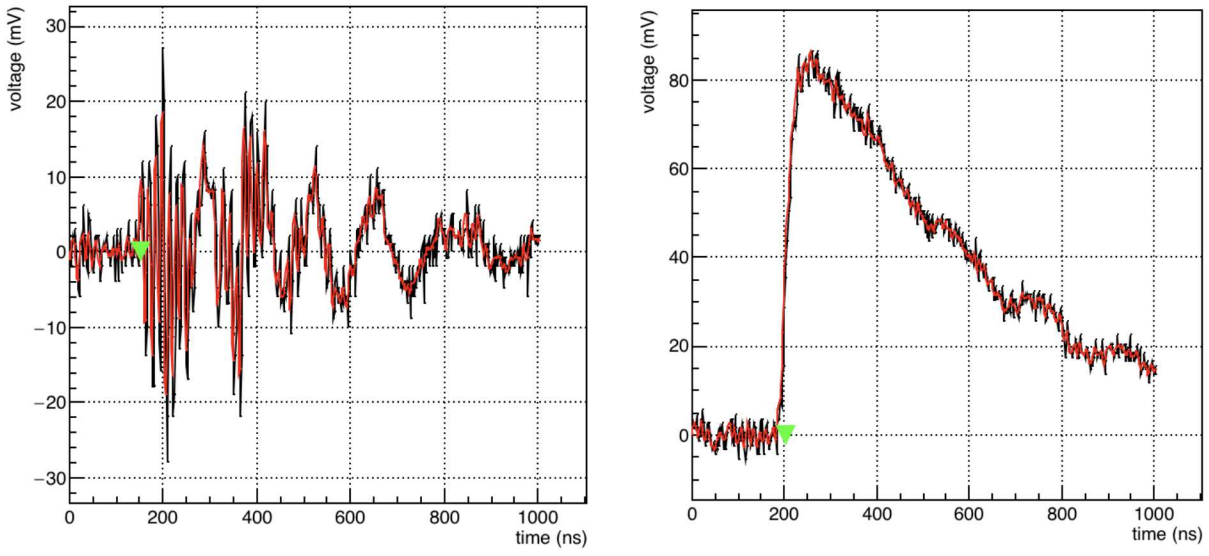

(a) (b)

Figure 3.5: Example waveforms with the SensL board readout in the shielded configuration. There is still a source of low-frequency noise (a), however the rate is low enough to push the trigger threshold down. The high frequency noise observed previously is absent (b).

Energy Response

The energy response was characterized by acquiring data with a Na-22 source in the same configuration described for the PMT measurements. Figure 3.6 shows the energy spectrum for the un-shielded configuration in black. As described above, due to the electronic pickup presumably caused by the jumper wires, the data acquisition trigger rate was too high for normal operation unless the threshold was raised to approximately a 200 keVee level. In addition, noise not removed by signal processing contributes to non-physical features in the lower-end of the energy spectrum. In the same figure, the spectrum in the shielded configuration is shown in red.

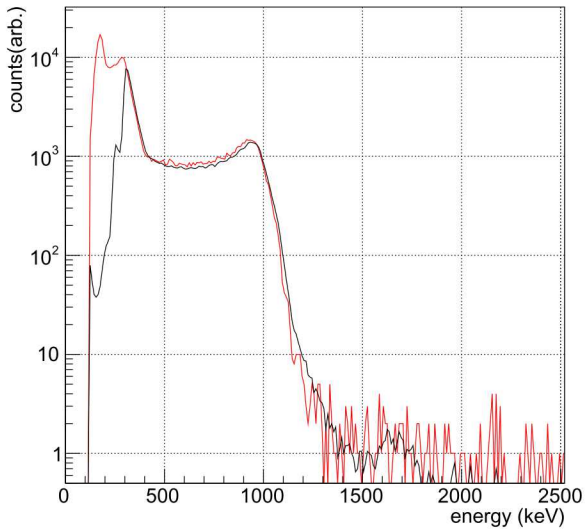

Figure 3.6: The energy spectrum from the SensL readout from a Na-22 source in the shielded (red) and unshielded (red) configurations. The high trigger threshold necessary to obtain a reasonable event rate due to electronic noise in the unshielded configuration is visible at approximately 200 keVee.

Particle Identification

The pulse shape discrimination as a function of energy for the SensL array and summing board is shown in Figure 3.7a. The noise problems described above results in an additional software threshold after a PSD cut at about 350 keVee. This is too high to see the 340 keV Compton edge from 511 gamma particles. The FoM for the SensL readout at 2000 keVee is 3.0, and drops to 1.4 at 500 keVee.

In the shielded configuration, the threshold on the PSD did lower, as shown by Figure 3.7b, however the FoM did not improve at lower energies and in fact is lower at higher

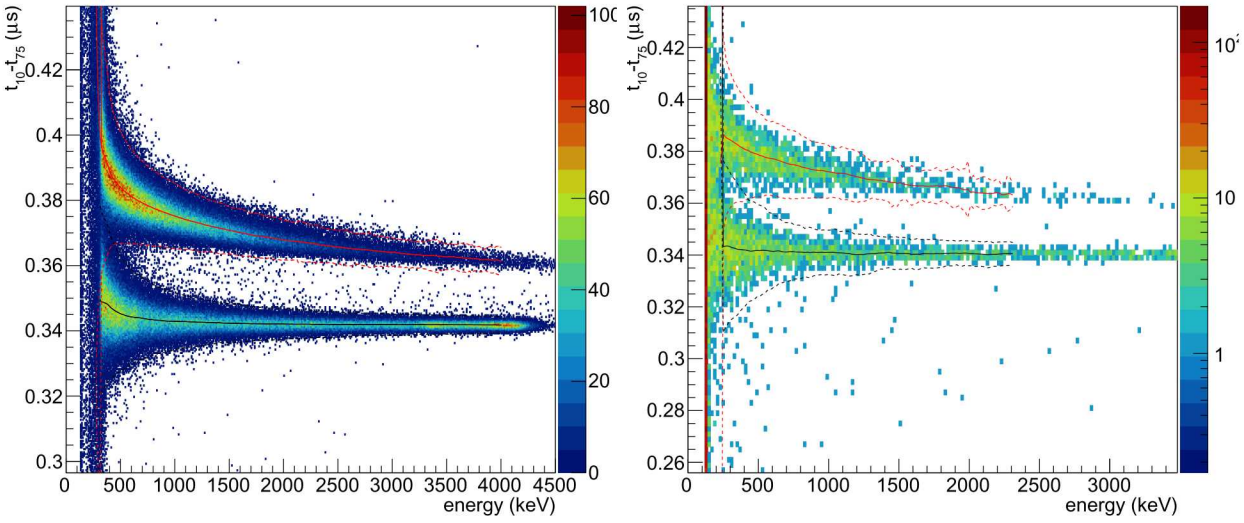

(a) (b)

Figure 3.7: (a) The pulse-shape discrimination calibration for the SensL array in the unshielded configuration. (b) The PSD parameter as a function of energy for SensL's summing board in the shielded configuration.

energies: at 500 keVee the FoM is 1.4, and at 2000 keVee the FoM is 2.4. This is likely inflated by poor statistics for the later case.

Timing Response

The timing response of the board was measured in the same fashion as before. Two 2" stilbene crystals coupled to Hamamatsu's H1949-50 2" photomultipliers were placed 2.5" apart, and 10" away from the stilbene crystal coupled to the ArrayX-BOB6_64S Summing Board. A ^{22}Na source was placed equidistant between the two. Figure 3.8 shows the coincidence between gamma particles without any PSD cut applied (in order to avoid the high threshold after the PSD cut). The timing resolution of the SensL readout is evaluated at 1.12 ns, a significant reduction in performance compared to the PMT readout, and greatly reduced compared to the expected performance of a single SiPM.

Figure 3.9 shows the timing difference between the SensL summing board output and PMTs A and B. The timing resolution evaluated using Equation 2.4 is 1.51 ns, compared to 1.12 ns without the shielding. It should be noted that the transit-time spread (TTS) of C-series SiPM are expected to be between 200-400 ps. If each of all 64 SiPM were independent measurements that contributed equally to the summed waveform, the expected timing would be

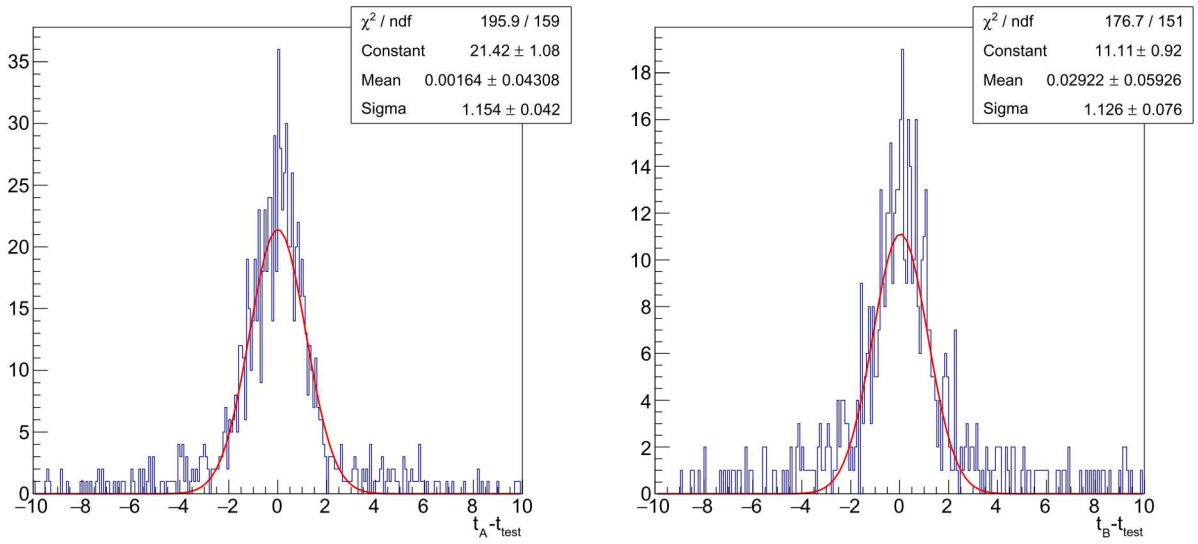

(a) (b)

Figure 3.8: The time difference between (a) the SensL summing board readout compared to H1949-50 A and (b) the SensL summing board readout compared to H1949-50 B.

$$\sigma_t^{sum} = \sigma_t^{ind.}\sqrt{64} = 8\sigma_t^{ind}. \tag{3.1}$$

For 200-400 ps TTS on an individual SiPM, the summed response would be 1.6-3.2 ns. However, all 64 SiPMs in the array are not expected to contribute equally: there may be a handful of SiPMs that dominate the pulse. This warrants further study to determine whether, for example, the timing response would improve by only reading out a handful of pixels for a timing measurement, and all for an energy measurement. FY19 measurements utilizing our pixelated board readout will explore this.

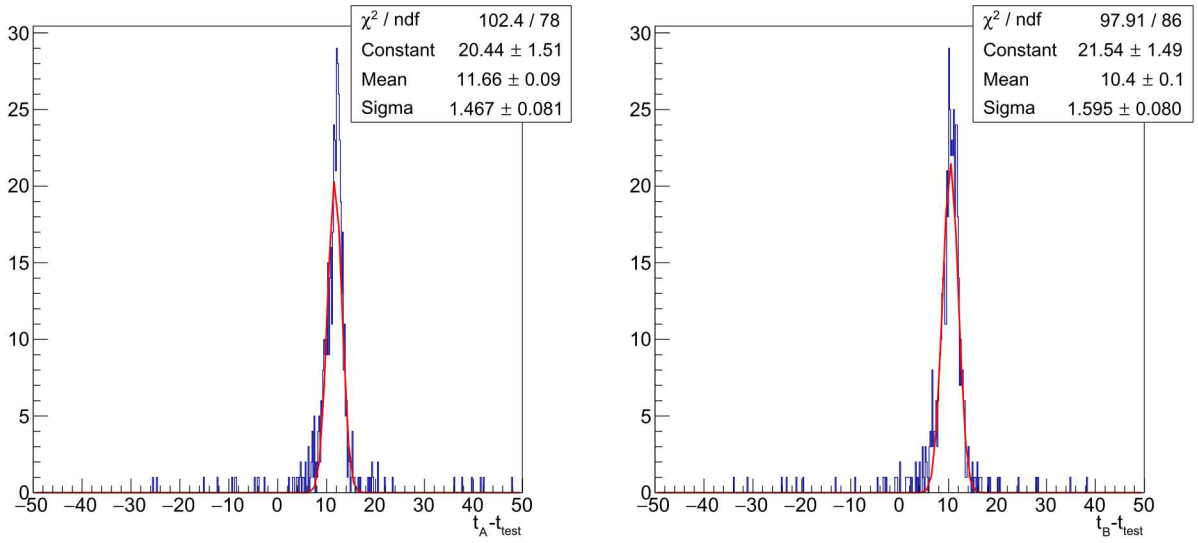

(a) (b)

Figure 3.9: The time difference between (a) the shielded SensL summing board readout compared to H1949-50 A and (b) compared to H1949-50 B.

Chapter 4

SNL's summing board

Based on our experience with SensL's out-of-the-box solution for summing their 64 channel array, the performance of any neutron imaging system reliant on timing and pulse shape discrimination will have degraded performance with this readout compared to a photomultiplier tube, depending on the system. The timing resolution degrades from 288 ps to 1.12 ns, and the FoM at 500 keVee from 1.7 to 1.4. It is not clear from our studies whether the electronic noise is the major cause of the PSD and timing degradation, and future studies will be performed with additional shielding to reduce this effect. Regardless, the size of the SensL summing board and it's out of the box performance make it impractical for a PMT replacement as is.

In an effort to improve the timing response, we have designed a board and compared it's PSD performance to SensL's summing board. All characterizations were performed with the assembly inside the mu-metal box for shielding. The design goals, electronics performance and testing, and conclusions of the effort are described in Appendix A. Example scintillation pulses are shown in Figure 4.1. The timing response is significantly slower than that of the SensL summing board and some additional noise problems are apparent. These will be addressed in Appendix A. The energy response to ^{22}Na coupled to a 2" stilbene crystal is shown in Figure 4.2, and the PSD response is shown in Figure 4.3. The response of either the board or our data acquisition system saturates at about 1200 MeVee, so we are unable to characterize the FoM at 2000 keVee. However we are able to fit the PSD at 500 keVee, and the FoM has degraded significantly compared to SensL's board: 0.92 compared to 1.4. This would likely be improved by design iterations, see Section A.6.3 for a discussion of the timing response of this board.

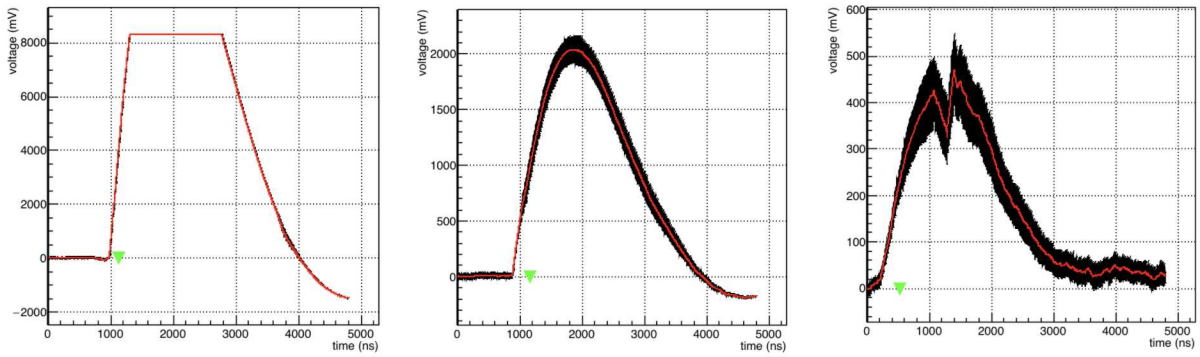

(a) (b) (c)

Figure 4.1: Example waveforms from SNL's summing board readout: (a) a saturated pulse (b) a nominal waveform (c) effect not fully understood. All waveforms have a ∼500 MHz noise that is filtered out during signal processing (the red curves are post-filtering).

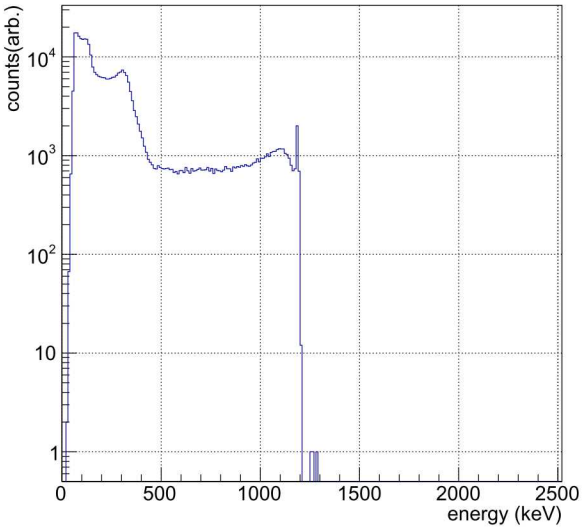

Figure 4.2: The energy spectrum from a ^{22}Na source readout with the SNL summing board

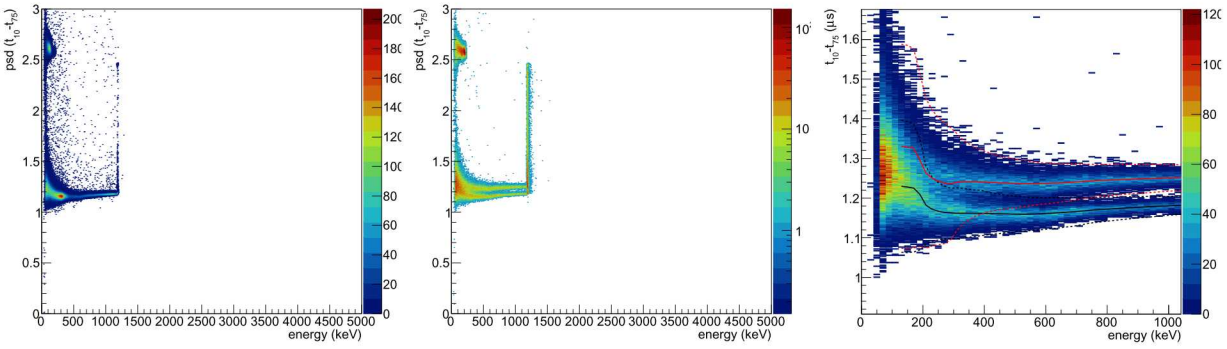

(a) (b) (c)

Figure 4.3: The pulse-shape discrimination readout with the SNL summing board from a (a) ^{22}Na source and (b) AmBe source. The calibrated PSD response with the mean and standard deviation for the neutron and gamma bands is shown in (c), with the neutron trends in red and the gamma response in black.

Chapter 5

Discussion and Conclusion

Based on the results presented here, we have found the best PSD and timing response with SensL's 8x8 C-series array is from a passive sum much like the summing board offered by the manufacturer. See Figures 5.1-5.3 for comparisons between the PMT readout and the SensL summing board readout. Noise and feedback from the fast amplifiers that we first tried caused us to use slower, more well behaved amplifiers, but these did not perform well compared to a simple passive sum. The results of the timing and PSD performance are summarized in Table 5.1. Although the timing was found to be not as good as the PMT response, the PSD is comparable. The timing response may be limited by statistics: the sum of 64 equally contributing and independent measurements with a 200 ps resolution is 1.6 ns. While it is not clear that all pixels in the array contribute equally, this may limit timing performance and motivate summing a smaller subset of pixels for a timing measurement independent of the summed response used for energy response. It should also be noted that the J-series array from SensL has improved timing response on the individual SiPM level. Testing other faster SiPM arrays will be conducted in follow-on work.

It should be noted that, without the size constraints, the performance would be acceptable for some systems. The MINER system [8] is limited to the single photon transit time spread of the photomultiplier used (ET9821B), approximately 1 ns (σ). However, other systems such as correlated neutron-gamma measurements require much better timing resolution.

In terms of power output, an 8x8 array of 6x6 mm^2 C-series SiPM is expected to draw $O(100)$ μW for a 2.5V over voltage compared to $O(100)$ mW of the H1949-50 operating at 2000 V. The J-series is expected to draw approximately half the current of C-series. SiPM replacement of PMTs is still well-motivated by the many benefits of SiPMs, and while there is room for improvement in the timing response, both the timing and PSD response are

Configuration	FoM (500 keVee)	FoM (2000 keVee)	σ_T (ns)
H1949-50	1.7	2.95	0.288
SensL	1.4	3.0	1.12
SensL shielded	1.4	2.4	1.51
SNL board shielded	0.92	-	-
MINER system			$O(1)$

Table 5.1: Performance parameters for each configuration.

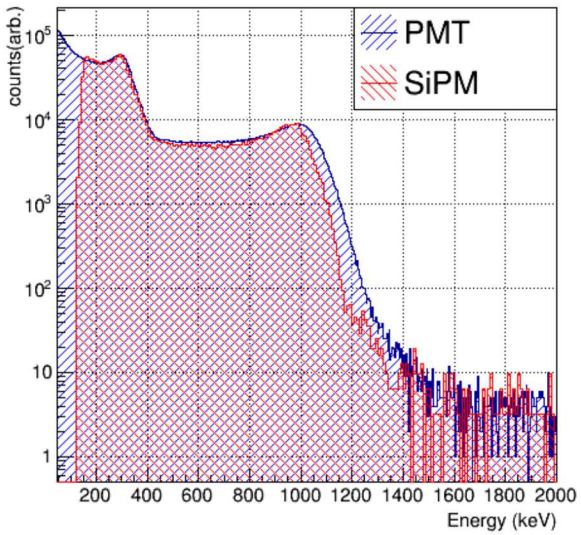

Figure 5.1: A comparison between the PMT readout and SiPM readout of a 2" stilbene crystal

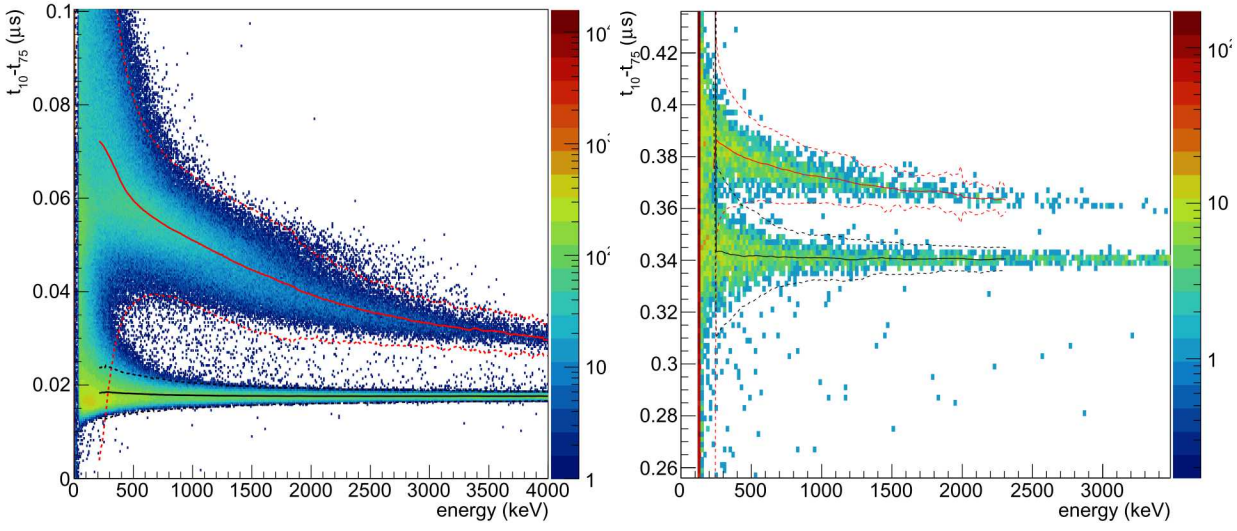

(a) (b)

Figure 5.2: A comparison of the PSD response from the PMT readout (a) and SiPM readout (b).

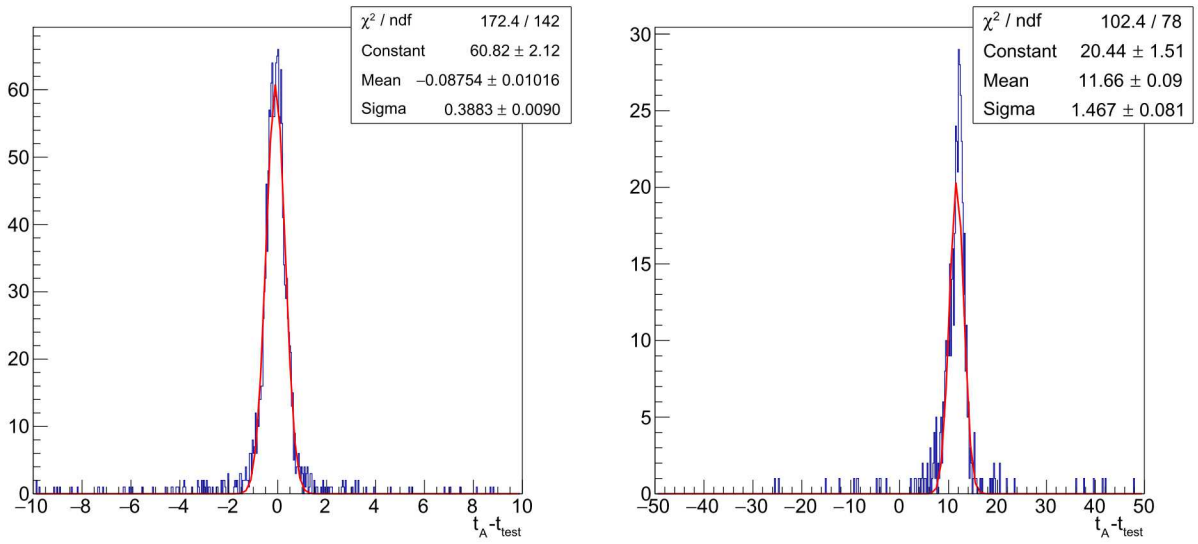

(a) (b)

Figure 5.3: A comparison of the timing response from the PMT readout (a) and SiPM readout (b).

comparable to some neutron imaging systems that rely on coincident neutron scatters (e.g. the MINER system). The outstanding issue is the physical size of SensL's summing board. This will be addressed in future work by laying out a passive summing board based on SensL's circuit, but on a smaller footprint. Hamamatsu is another manufacturer that offers SiPMs with close to half the capacitance and noise as SensL's J-series. This may translate to less noise issues and improved PSD and timing compared to the C- and J- series SiPMs. We will explore these options in the next FY for implementation into an imaging system. Another revision of the active summing solution could be pursued, however that path appears to be higher risk for implementation into a larger system.

Appendix A

A.1 SiPM replacement for PMT Objectives

A.1.1 Summed SiPM Array

The objective of this effort is to evaluate the potential to substitute Silicon Photo-Multipliers (SiPMs) for Photo-Multiplier Tubes (PMTs). SiPMS have definite advantages in terms of size and their bias voltage is significantly lower than PMTs. The SensL devices tested require only 25V to 29V of bias voltage as compared to 750V to 1000V typically required by a PMT. The disadvantage of a SiPM are small active area size, higher dark current noise, and larger capacitance.

The scintillator being used is a stilbene crystal approximately 2 inches in diameter. Pulse shape discrimination can be used to discriminate between gamma-rays and neutron particles in stilbene crystals. To do this requires a large active area and a photo-detector with a fast response. To achieve the active area necessary, an array of SiPMs must be used. All the SiPM outputs must be summed together. Using high speed design practices is necessary to preserve the shape of the scintillation light decay to achieve pulse shape discrimination.

To achieve low noise performance and allow easy interface to data collection equipment, a pre-amplifier is required. For convenience purposes, it is desirable to have a pre-amplifier board that runs on a single supply voltage along with a circuit that provides the SiPM bias voltage. The design considerations for a pre-amplifier board that meet these requirements are contained in subsequent sections.

A.1.2 SiPMs Under Test

The SiPMs chosen for testing are SensL P/N MicroFC-60035-SMT-TA. This is the largest SiPM SensL produces, but at 6mm x 6mm square, it is still small compared to the 2" diameter PMTs used on scintillators. A schematic symbol showing connections and suggested biasing for the SensL SiPM are shown in Figure A.1 Key specifications for interfacing to this device are:

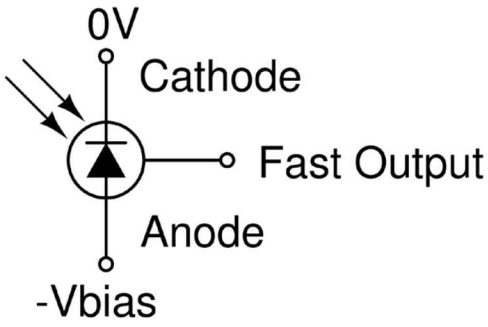

Figure A.1: SensL SiPM Connections [9].

MicroFC-60035 Key Specifications		
Breakdown Voltage (Vbr)	24.2V min.	24.7 max.
Overvoltage	1.0V min.	5.0V max.
Anode to Cathode Capacitance	3400pF typ.	

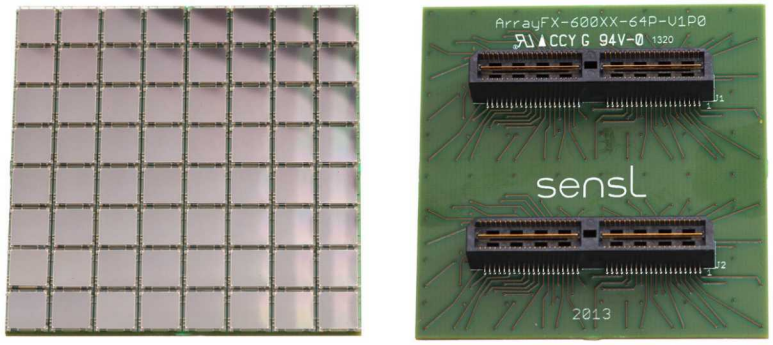

Figure A.2: SensL 8x8 array [10].

These devices are available from SensL as a prepackaged, 8x8 element array (see Figure A.2. This pre-packaged array was chosen to reduce fabrication costs and to allow flexibility in the type of SiPM used in future experiments. Interface to the individual SiPMs is provided through the use of two 80-pin connectors on the back side of the board. Anode and Fast Output terminals are individually available on the connectors, but all 64 Cathodes are tied together to a set of common pins on the connectors.

A.2 Design Derivation

A.2.1 SensL Standard Output

The design used to interface to the SiPM standard output is based on SensL's example readout circuit shown in Figure 3. This is a transimpedance amplifier which converts a

current waveform into a voltage waveform. Initial component values chosen were as recommended by SensL with the following exceptions:

1. U1 was changed from a Texas Instruments OPA656 to a Linear Technology LT6268-10. The primary reason was to achieve as fast of a response as possible. The OPA656 has a 230MHz gain-bandwidth product whereas the LT6268-10 has a 4000MHz gain-bandwidth product. Both devices are specified for use as photodiode transimpedance amplifiers.

2. R2 was initially set to 0 ohms because a separate buffer amplifier is placed after U1 to drive coaxial cable. The buffer amplifier chosen is a maximum MAX4201EUK. It was chosen because it is specified to drive long lengths of coaxial cable and has a 50ohm output impedance to match a CAEN digitizer's 50ohm input impedance.

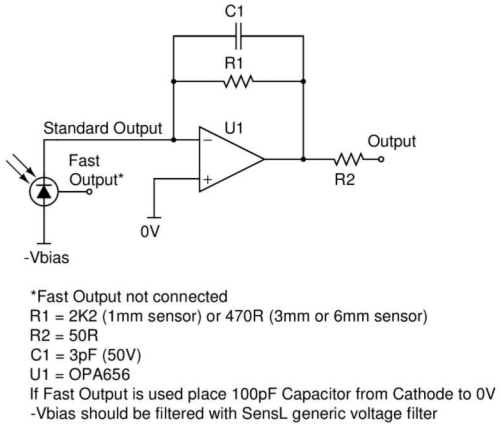

Figure A.3: SensL example readout circuit [9].

All of the SiPM anodes were connected to select resistors that were in turn connected to a single, negative bias voltage. This allows the selective connection of as many or few of the SiPMs into the summing amplifier as desired. See A.5 for further information.

A.3 SensL Fast Output

The design used to interface to the SiPM Fast Outputs is based on SensL's example readout circuits shown in Figure A.4 and A.5. The circuit in Figure 5 depicts the same Standard Output as Figure 3, except it includes recommendations for fast readout options. To achieve maximum flexibility, a transformer and an amplifier were connected in series to the Fast Output. By doing this, experimentation on either transformer coupled or amplified signals can be performed by simply replacing components with jumpers as desired. Further details are contained in A.5.

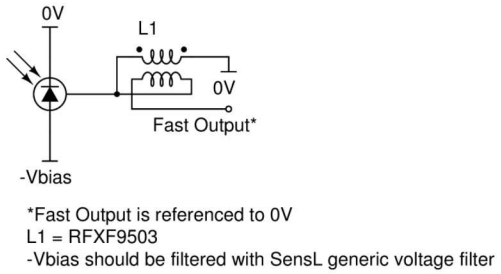

Figure A.4: SensL fast readout balun transformer circuit [9].

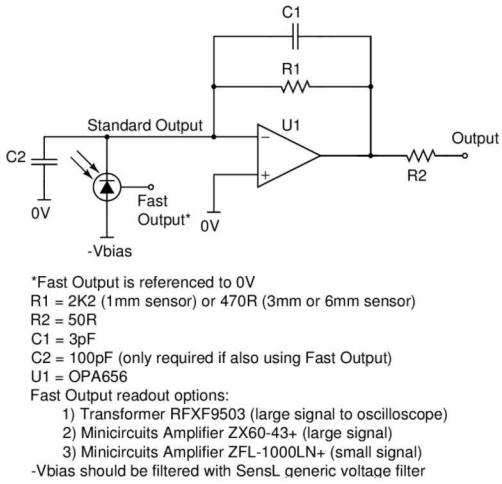

Figure A.5: SensL example dual readout circuit [9].

A change from SensL's recommendation is the substitution of a Mini-Circuits RAM-6A+ instead of a ZX60-43+ or a ZFL-1000LN+. The reason for this is both recommended Mini-Circuits devices are pre-packaged amplifiers with a housing and SMA connectors. To allow all the circuits to be placed on a single circuit board, a Mini-Circuits RAM-6A+, which is a monolithic amplifier, was used along with supporting components. It is a compromise choice with a bandwidth between the ZX60-43+ and ZFL-1000LN+, but all the amplifiers have approximately the same gain in the 0.1 to 1000MHz region.

The layout and components chosen for the fast amplifier are as specified in Mini-Circuits RAM-6A+ evaluation board, P/N WTB-414-6A+ (4)

A.3.1 SensL Fast Output Summing

The circuit used to sum the fast outputs is based on the SensL Signal Driven Multiplexing circuit shown in Figure A.6. All of the Fast Outputs are summed together using a diode OR arrangement. To achieve very low forward voltage drop, the diodes are pre-biased in the forward conduction direction with a DC diode bias current.

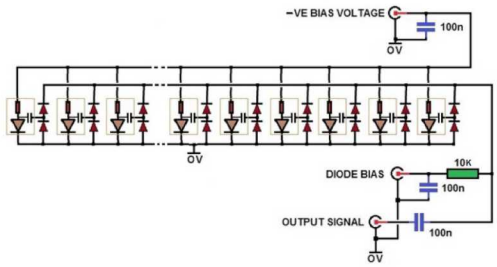

Figure A.6: SensL example dual readout circuit [9].

A.3.2 DC to DC converters

To realize a circuit board that requires only one power source, a number of supply voltages/currents had to be generated:

1. SiPM bias voltage, variable, between -24.0VDC and -29.0VDC
2. SiPM Fast Output summing diode bias current, variable, 0.8mA to 19.2mA
3. LT6268-10 power, +2.5VDC and -2.5VDC
4. DCR011205U power, +5VDC and -5VDC
5. RAM-6A+ power +6VDC

Switching power supplies are required to generate negative voltages from a single positive input voltage. In general, they also consume less power than linear regulators for positive voltages significantly different than the input voltage. The problem with switching power supplies is switching noise. To mitigate this, a low noise switching regulator is used for the +/-5VDC power. The Texas Instrument DCR01 series module chosen is comprised of a switching regulator followed by an internal low dropout linear regulator. Texas Instruments specifies noise for this device at 21mV peak to peak (6).

A.3.3 Driving CAEN Digitizers

High speed CAEN digitizers are used to capture the output waveforms. The CAEN digitizers have a 50ohm input impedance and are specified for +/-1V input signal range. To accommodate this, a Maxim MAX4201 buffer amplifier is used to buffer the SiPM standard output from the LT6268-10. This isolates the LT6268-10 from the capacitive loading of coaxial cables and the input of the CAEN digitizer which can cause stability problems.

The buffer provides an additional benefit in that it produces an effective gain of 0.5 due to its 50ohm output impedance coupled to the CAEN 50ohm input impedance. The LT6268-10 is a rail-to-rail output amplifier so its output can approach +/- 2.5V. By utilizing the MAX4201, this is converted to a range of +/- 1.25VDC which will not harm the CAEN digitizer input.

For the Fast Output, the Mini-Circuits RAM-6A+ has a 50ohm output and is specified to drive 50ohm coaxial cable and 50ohm input devices. It has a +6VDC supply and is capacitively coupled to the output which will yield a potential +/-3V output. Bench testing will determine if an in-line attenuator is required to limit the output voltage swing.

A.4 Block Diagram

A block diagram of the board is shown in Figure A.7.

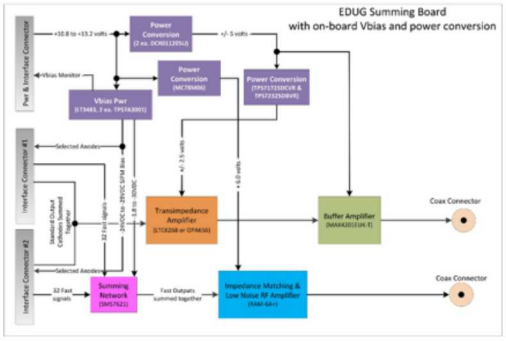

Figure A.7: Summing board block diagram.

A.5 Schematics, Layout and Photos

The schematic and layout of the Summing Board are contained in Appendix B. The board is 3 inches in diameter which was as small as could be reasonably made. The board is constructed with Rogers 4000 series substrate as specified by Mini-Circuits for use with RF amplifiers.(4) The design and layout were performed with high speed operation and noise suppression in mind. A shield layer and metal shield enclosures are used for critical components. Specifically, the LT6268-10 transimpedance amplifier and the Mini-Circuits RAM-6A+ are contained in a separate enclosure. The +/-5VDC switching converters are contained in a second, separate enclosure. The -35VDC switching converter used for the SiPM bias voltage is contained in a third, separate enclosure. Split planes and individual layers are used to keep power and grounds separated.

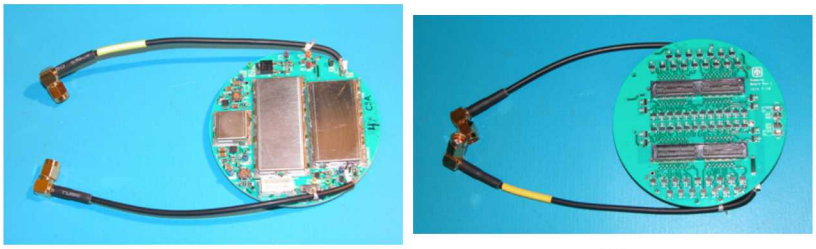

(a) (b)

Figure A.8: The summing board (a) top and (b) bottom.

A.6 Testing

A.6.1 DC to DC Noise

For the initial tests, a SiPM board was not connected and the inputs of the transimpedance and fast amplifiers were connected to ground. Switching converter noise present on the Standard Output is shown in Figure A.9a. Additional 0.01uF and 100uF capacitors were placed on the outputs of U4 and U6 and the shield ground was connected to signal ground near the output connector J1. This reduced the output noise from approximately +/-100mV peak to peak to approximately +/-50mV peak to peak. See Figure A.9b.

The level of noise present on the +/-5VDC supplies is significantly less than what is present on the J1 output. Opening the shield enclosure has no effect on the noise level. The posited reason for this much noise is due to capacitive coupling between the switching converter and the signal ground and signal layers on the board. This is despite the use of shielded enclosures, a shield layer and separate power/ground planes. This can only be solved by additional physical separation between the signal/ground layers and switching converters.

This level of noise was still too high so the on-board +/-5VDC switching converters were

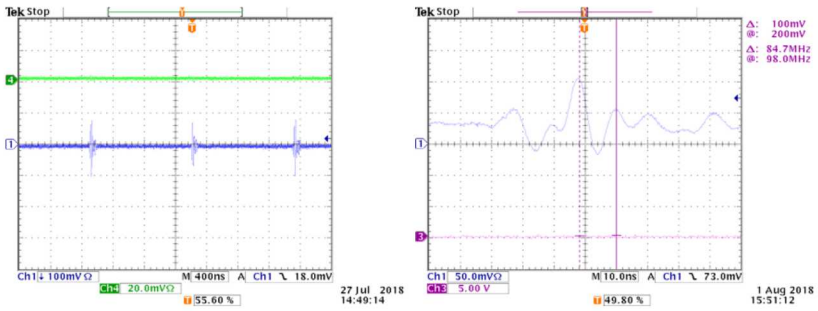

(a) (b)

Figure A.9: (a) Switching power supply noise present on the Standard Output, connector J1. (b) Switching power supply noise present on the Standard Output, connector J1 after additional output filtering was added.

disabled and external, filtered, +/-5VDC supplies were substituted. This reduced the noise to approximately +/- 20mV peak to peak. This noise is due to the switching noise associated with the SiPM Vbias switching converter. Additional filtering may help this in future board versions.

The conclusion from this is that there is not enough room on a single 3-inch diameter board to place both switching DC to DC converters and the low noise amplifiers. To maintain adequate separation with a 3-inch diameter form factor, a stacked, two-board implementation is suggested.

A.6.2 Dual Output

Testing revealed that dual outputs on a 64-element array is problematic using this design. The reason for this is the SiPM cathodes are all connected to the non-inverting input of the transimpedance amplifier used for the Standard Output. See Figure A.5. The Fast Output summing diodes are also connected to the cathode of the SiPMs. See Figure A.6. This results in the bias current of the summing diodes being conducted through the feedback resistor of the transimpedance amplifier. For dual readout of a few SiPMs, this is not a problem because the result of a DC bias current through the feedback resistor will be a negative DC offset of the transimpedance amplifier output. With a total of approximately 20 mA of summing diode bias current for 64 SiPMs and a 470ohm feedback resistor, 9.4volts of offset would be required from the transimpedance amplifier which is not possible. To implement a dual output, summed array, with a fast output summing diode array, a standard output circuit similar to the one depicted in Figure A.10 could be used.

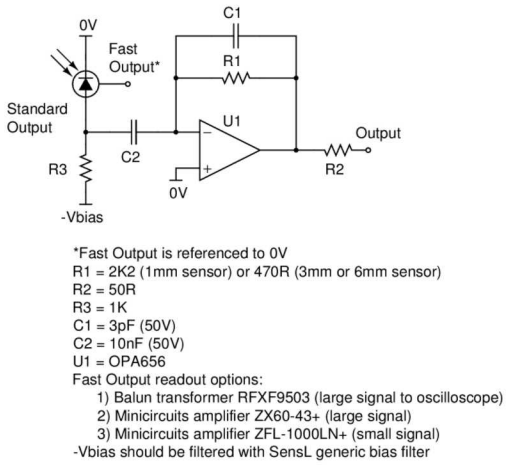

Figure A.10: SensL Example AC coupled dual readout circuit [9]

A.6.3 Standard Output Stability

A function generator set to output a square wave was connected to the input of the Standard Output amplifier chain through a series 100pF capacitor. The result is shown in Figure A.11a. Some ringing is present on the output which is mostly attributable to the ringing of the input waveform. At this point, the 64-element SiPM array was connected to the summing board. This caused instability in the Standard Output due to the additional capacitance connected to the transimpedance amplifier's input. See Figure A.11b. The capacitance of a SiPM is specified as 3400pF.(3) With a 64-element array, this sums to 218nF. While coupled to the summing board, the SiPM array, without a bias voltage applied, measured 285nF using a B&K model 889B LCR meter.

To achieve stability with the 64-element array attached, U1 was switched to a Texas Instrument OPA656 amplifier, C1 to 47pF and R1 to 4750 ohms. The output response to a square wave coupled through a 100pF series capacitor is shown in Figure A.11c. Clearly the speed has been greatly reduced, but this was a necessary tradeoff to achieve stability when the SiPM array was attached. A positive benefit i, noise has been reduced to less than +/-1mV peak to peak. See Figure A.11d. Because the OPA656 is a +/-5V part, the dynamic range of the output is now increased to approximately +/-2V.

Using the shielded enclosure and test configuration shown in Figure 18, noise measurements were recorded. With a 26.0VDC SiPM bias voltage, the resulting dark current noise is shown in Figure A.13. The SiPM array and summing board were set onto a 2" dia. by 2" CsI crystal inside the shield box. The resulting Standard Output pulses from background radiation are shown in Figure 22 A.17.

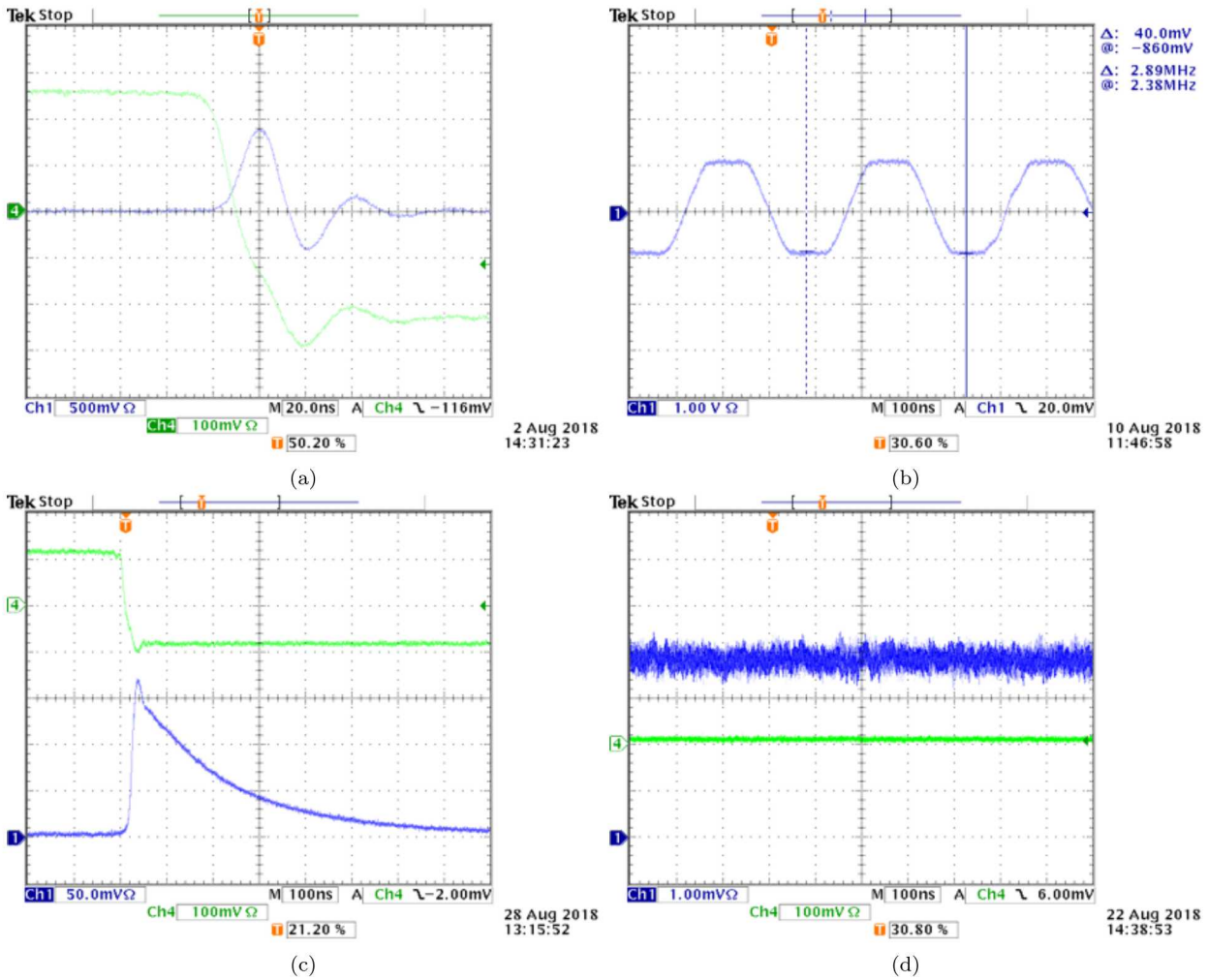

Figure A.11: (a) Standard Output pulse response using square wave generator through a 100pF series capacitor input. Ch4 (green) trace is the input waveform and Ch1(blue) trace is the output. (b) Oscillations with LT6268-10 amplifier Standard Output with SiPM array connected. (c) Standard Output with OPA656 and revised feedback components. (d) Standard Output noise (Ch 1, blue trace) with OPA656 and revised feedback components.

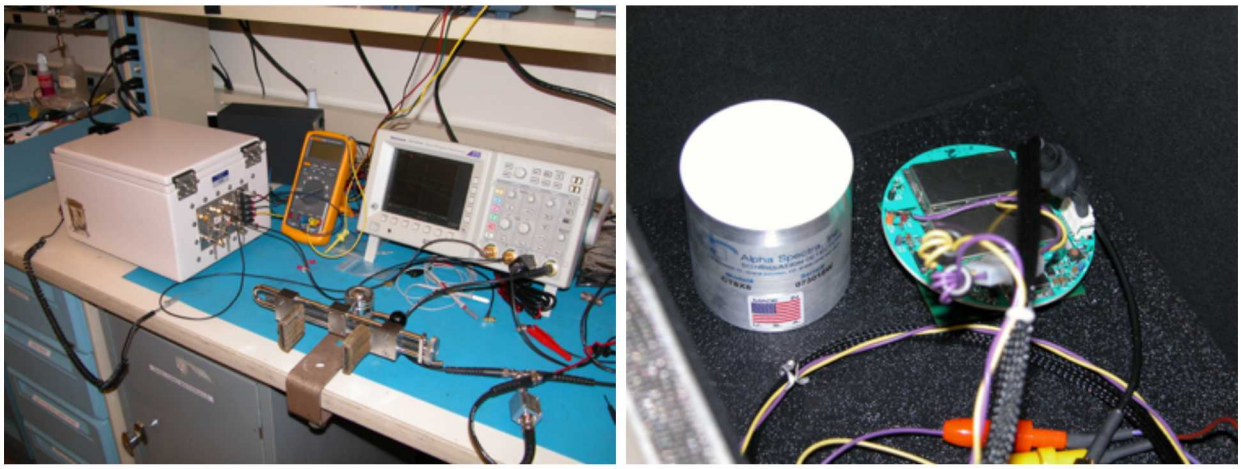

(a) (b)

Figure A.12: (a) Test configuration for measurements with the SiPM array. (b) Summing board coupled to SiPM array next to CsI crystal in shield box.

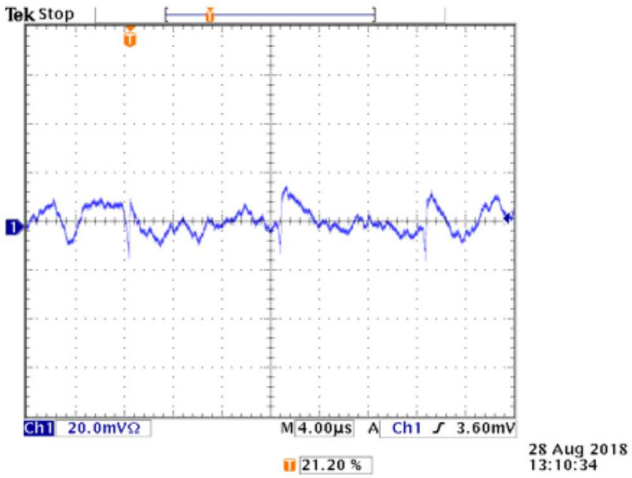

Figure A.13: 64-element SiPM array Dark Current noise with a 26.0VDC bias voltage.

Figure A.14: 64-element SiPM array with a 26.0VDC bias voltage coupled to the CsI crystal inside the shield box.

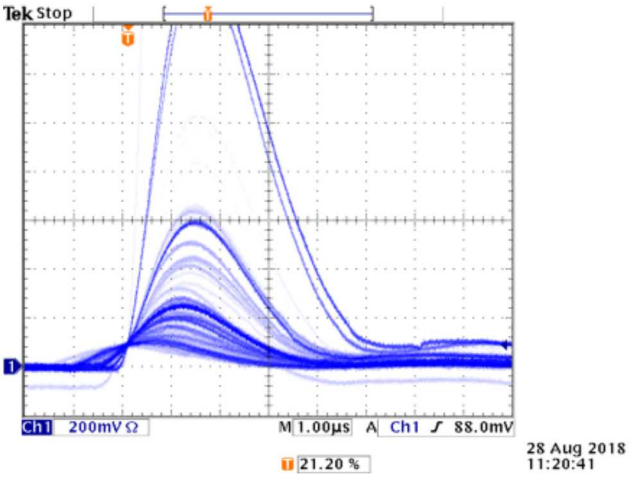

Figure A.15: 64-element SiPM array with a 26.0VDC bias voltage coupled to a CsI crystal. Output pulses are from background radiation.

A.6.4 Fast Output Stability

A limited amount of time was spent testing the Fast Output. Results similar to the LT6268-10 transimpedance amplifier resulted. The J2 output could be made quiet and stable, but when the array was attached the output oscillated.

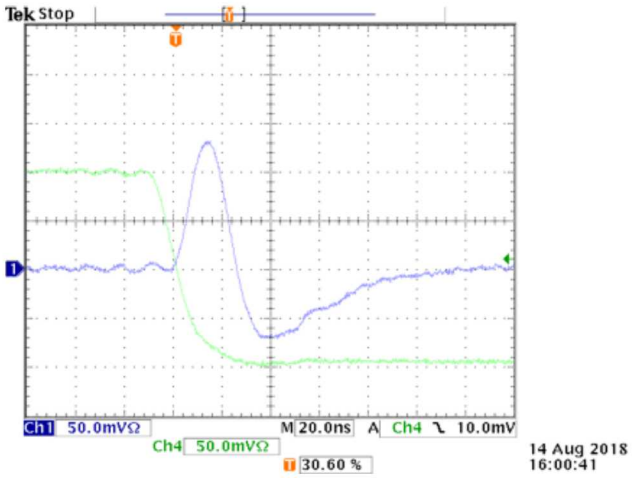

Figure A.16: Fast Output pulse response with a square wave input coupled through a 100pF series capacitor. No SiPM array is attached.

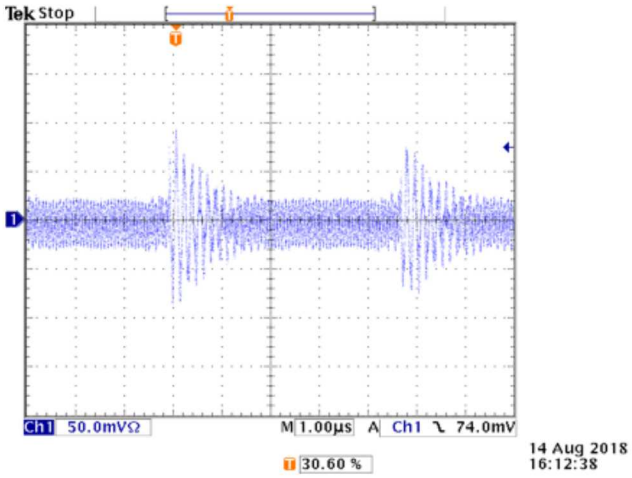

Figure A.17: Summing board Fast Output array noise and low-level oscillation when coupled to a SiPM array

A.7 Conclusion

Using a single amplifier on the SiPM 64-element array standard output may not produce the speed necessary for use in stilbene pulse shape discrimination. A single transimpedance

amplifier coupled to each element followed by a fast, summing, voltage amplifier may be required. Dual outputs are possible with a different circuit topology. The impact on speed and noise have not been analyzed. For lower speed application like CsI, a single transimpedance amplifier topology will work with a 64-element SiPM array.

Appendix B

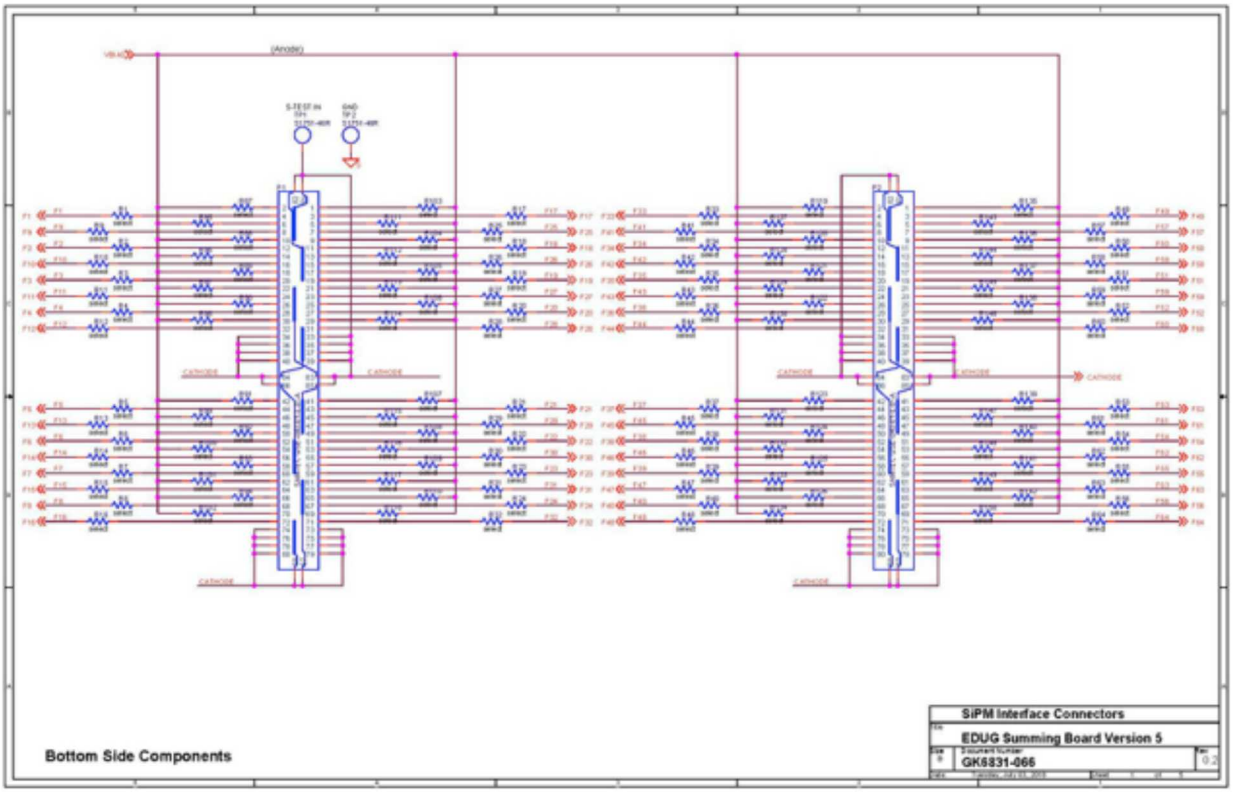
(Anode)
CATHODE
Bottom Side Components
SiPM Interface Connectors
EDUG Summing Board Version 5
GK9331-066

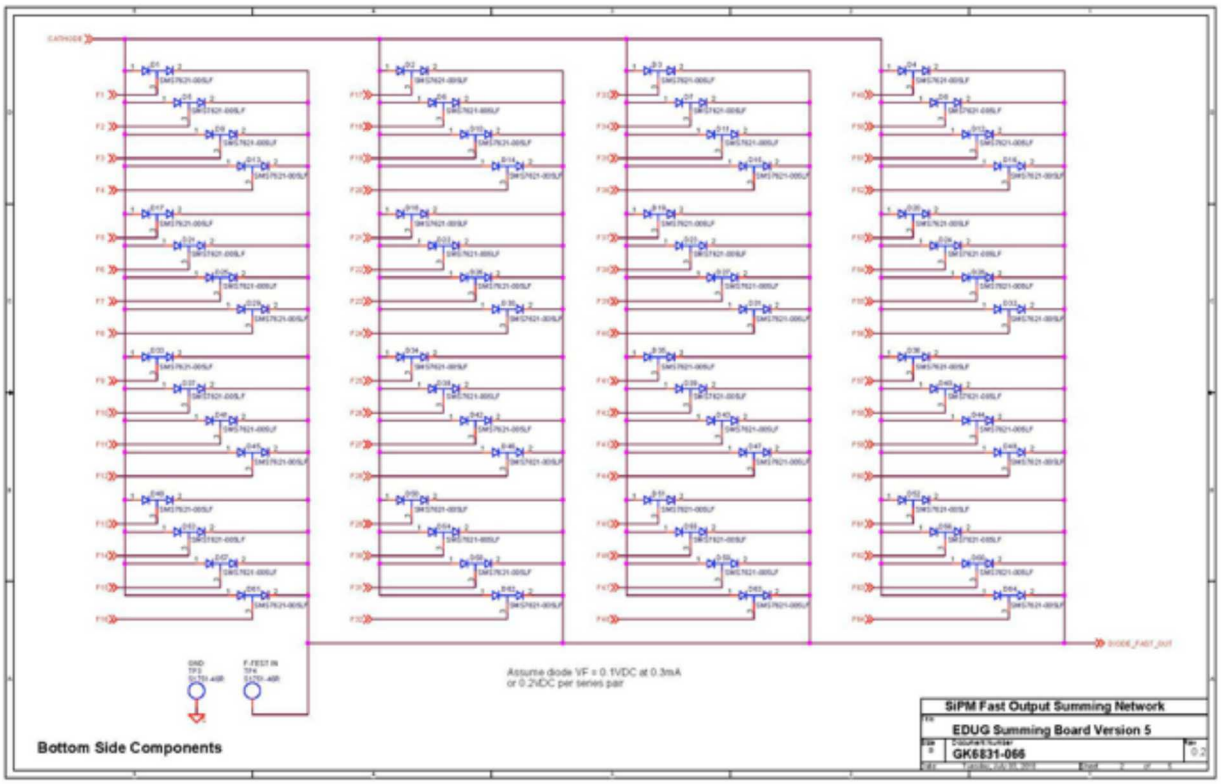
Assume diode VF = 0.1VDC at 0.3mA
or 0.2VDC per series pair
Bottom Side Components
SiPM Fast Output Summing Network
EDUG Summing Board Version 5
GK6831-066

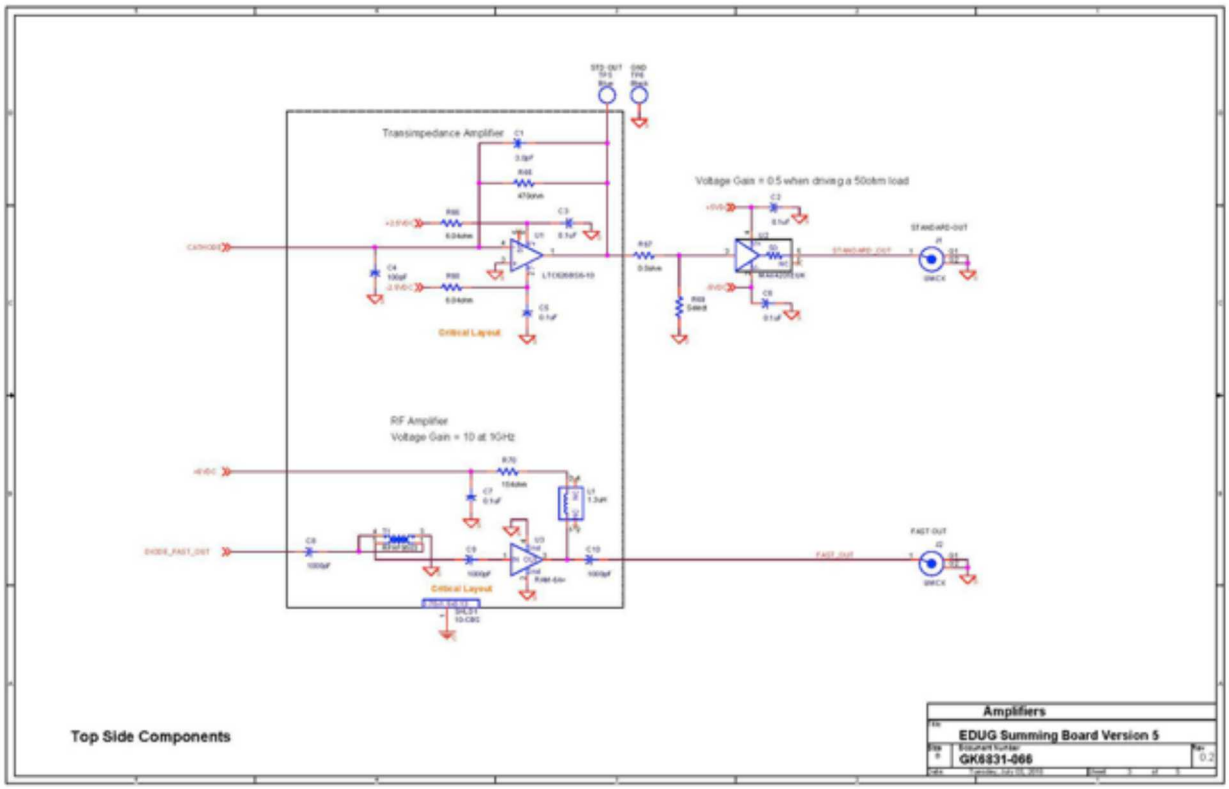
Transimpedance Amplifier
Voltage Gain = 0.5 when driving a 50ohm load
RF Amplifier
Voltage Gain = 10 at 1GHz
Critical Layout
Top Side Components
Amplifiers
EDUG Summing Board Version 5
GK6831-066

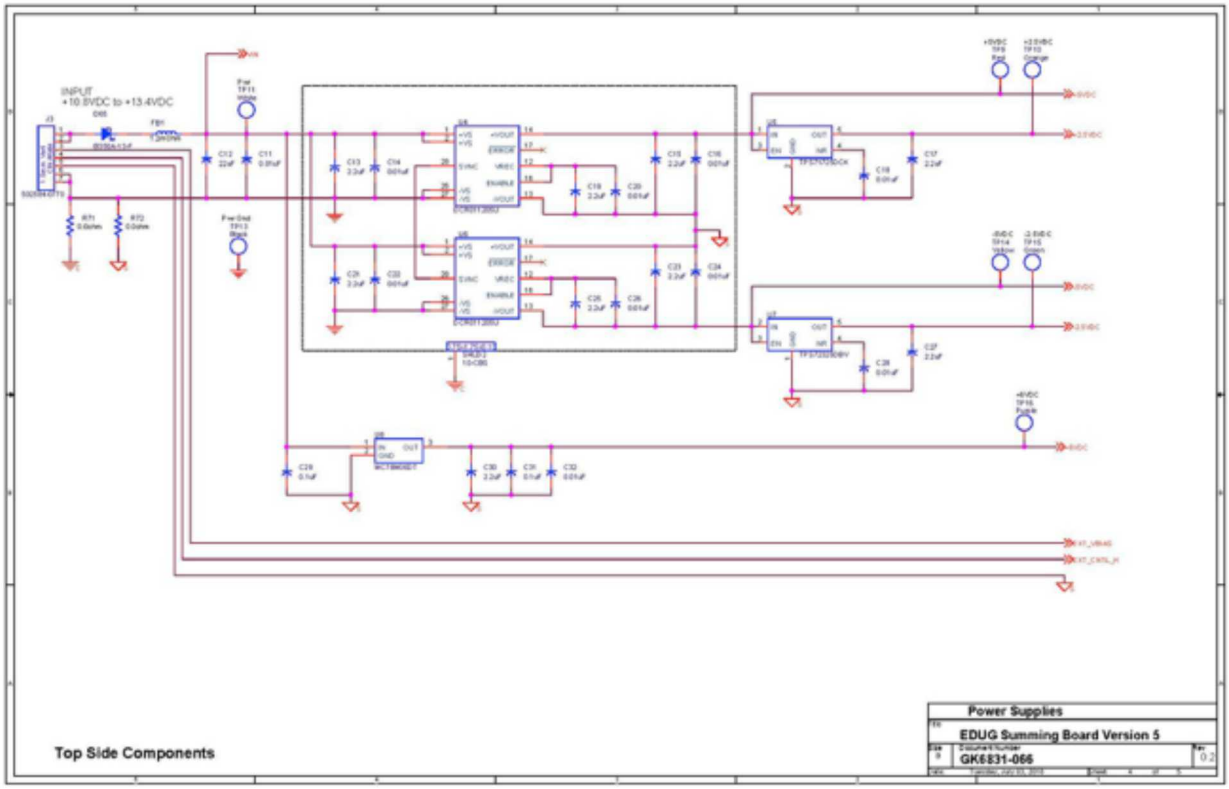
INPUT
+10.8VDC to +13.4VDC
Top Side Components
Power Supplies
EDUG Summing Board Version 5
GK6831-066

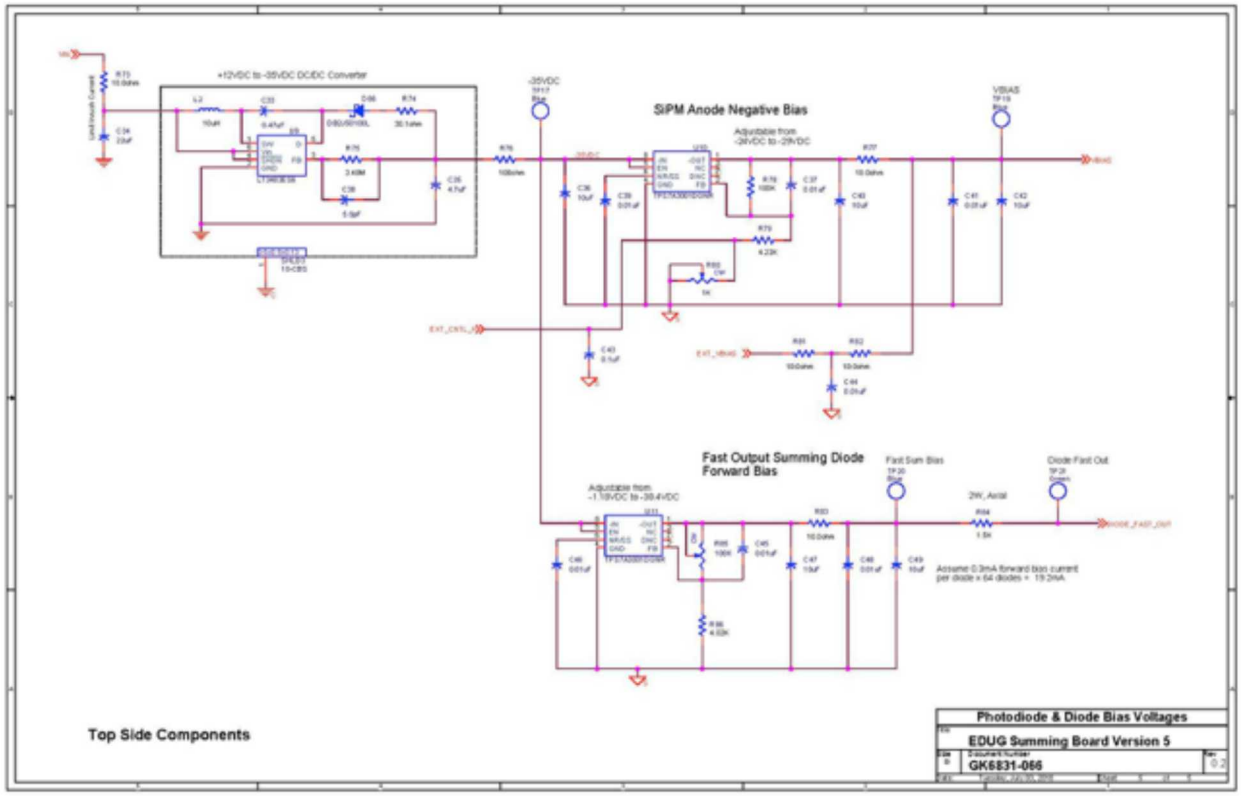
+12VDC to -35VDC DCIDC Converter
-35VDC
SiPM Anode Negative Bias
Adjustable from
-24VDC to -29VDC
VBIAS
Fast Output Summing Diode
Forward Bias
Adjustable from
-1.19VDC to -38.4VDC
Fast Sum Bias
Diode Fast Out
2W, Axial
Top Side Components
Photodiode & Diode Bias Voltages
EDUG Summing Board Version 5
GK6831-066

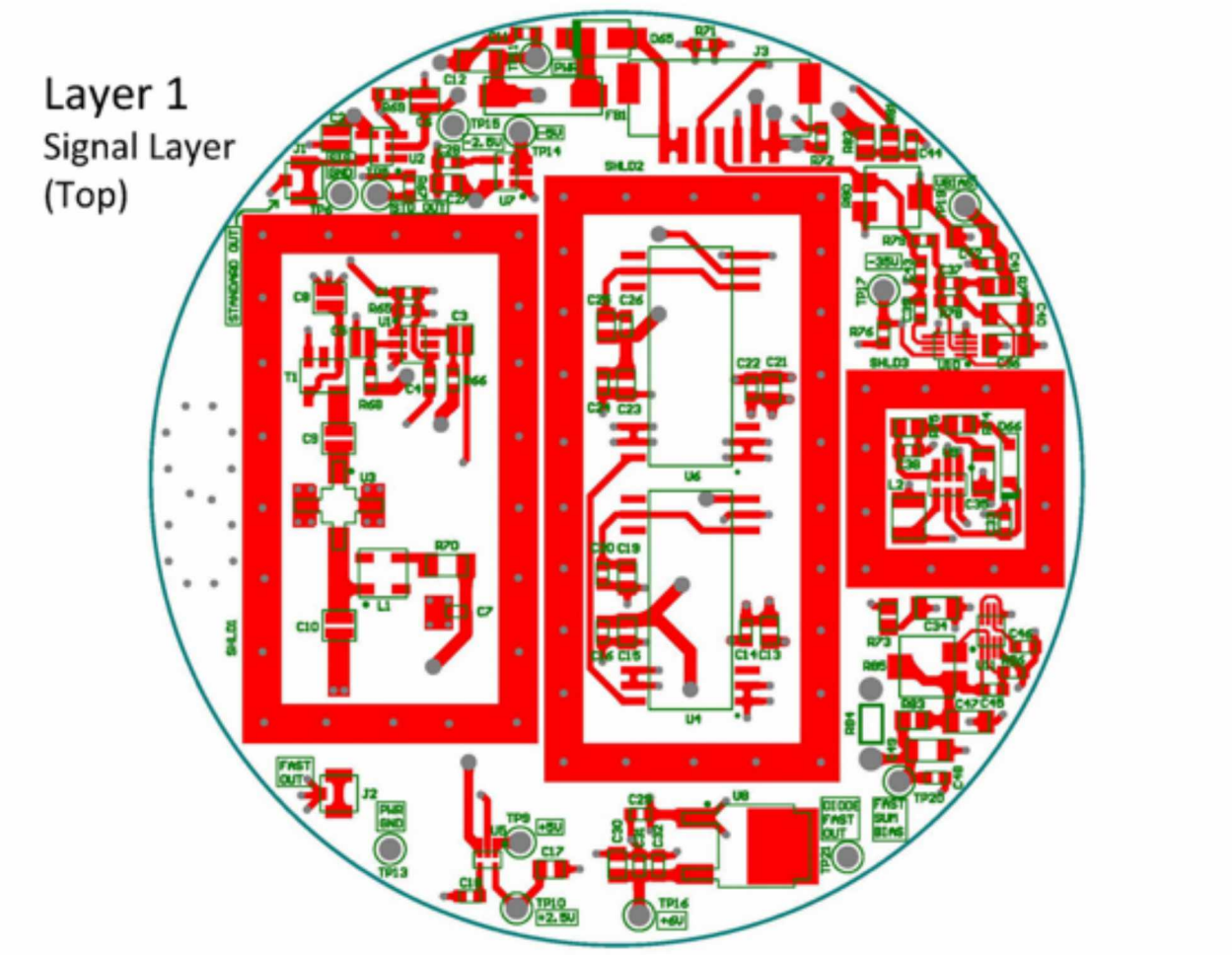
Layer 1
Signal Layer
(Top)

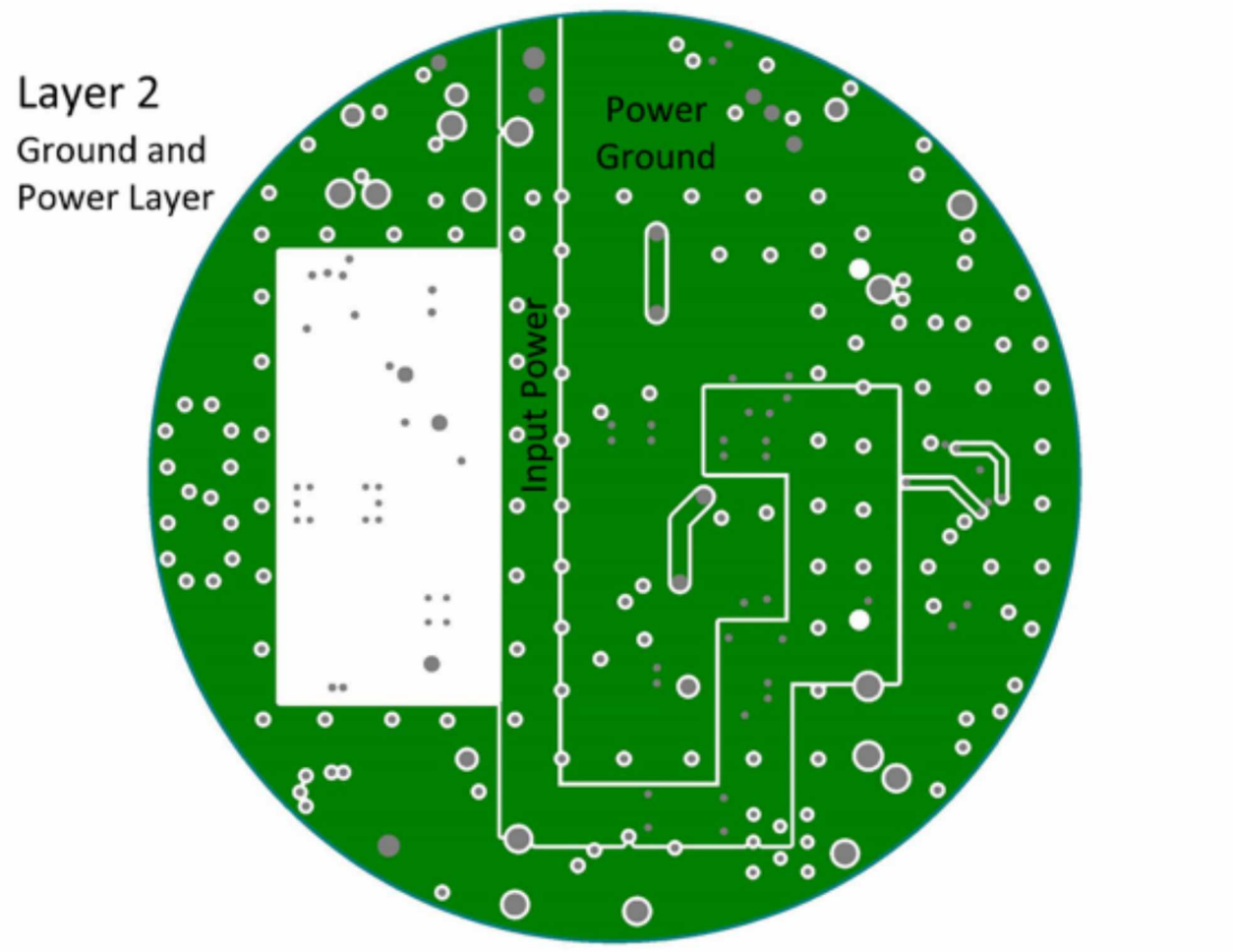
Layer 2
Ground and
Power Layer
Power
Ground
Input Power

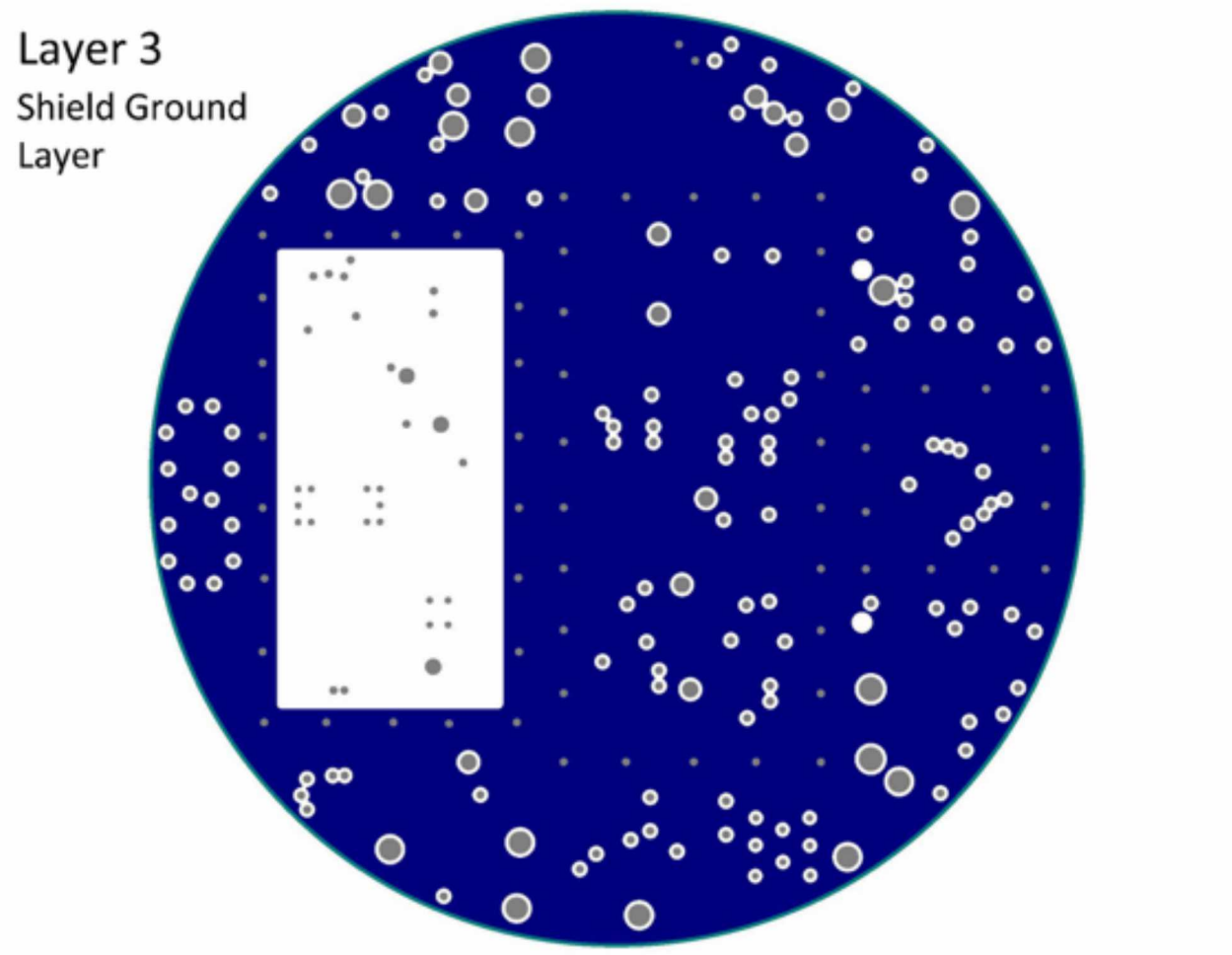
Layer 3
Shield Ground
Layer

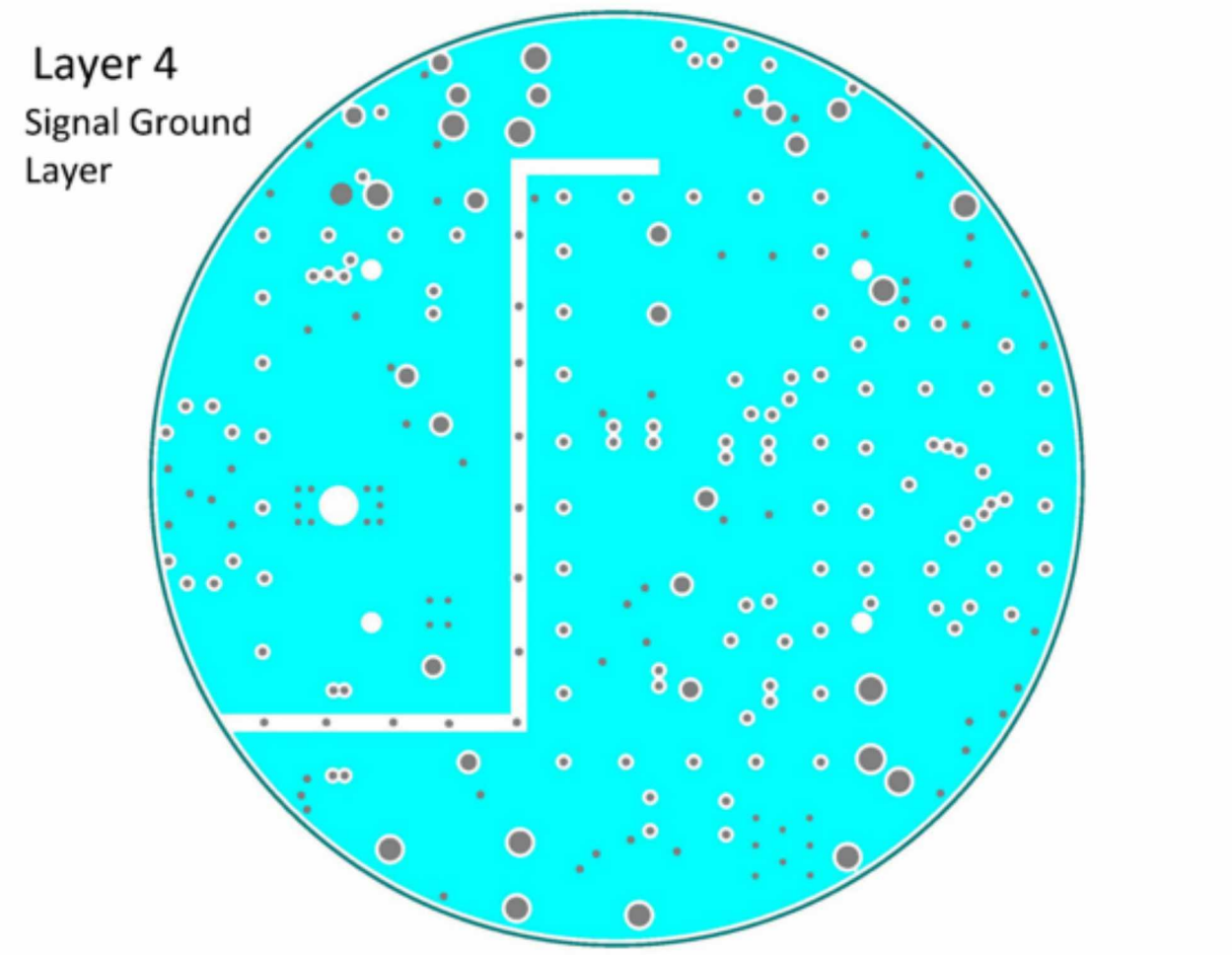
Layer 4
Signal Ground
Layer

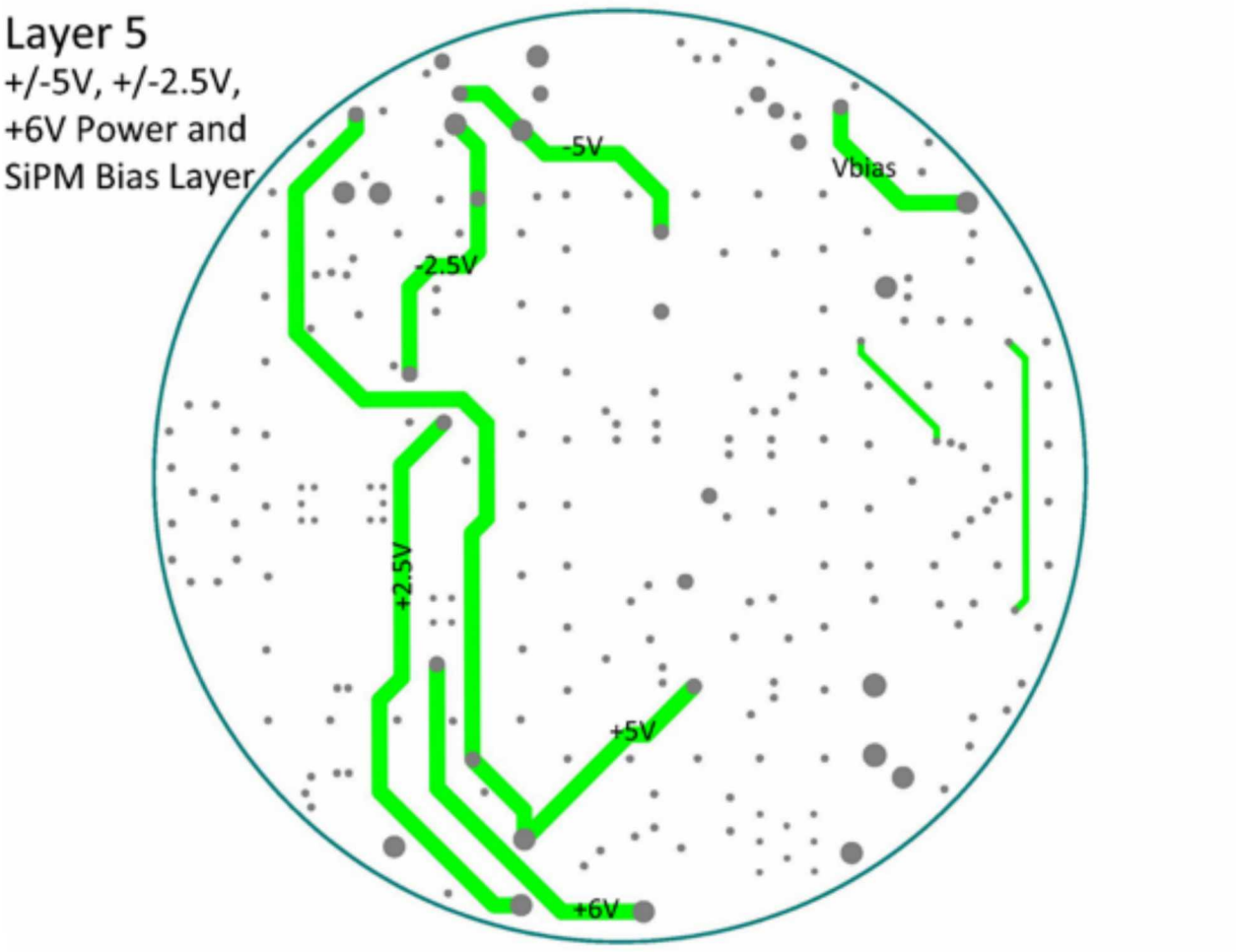
Layer 5
+/-5V, +/-2.5V,
+6V Power and
SiPM Bias Layer
-5V
Vbias
-2.5V
+2.5V
+5V
+6V

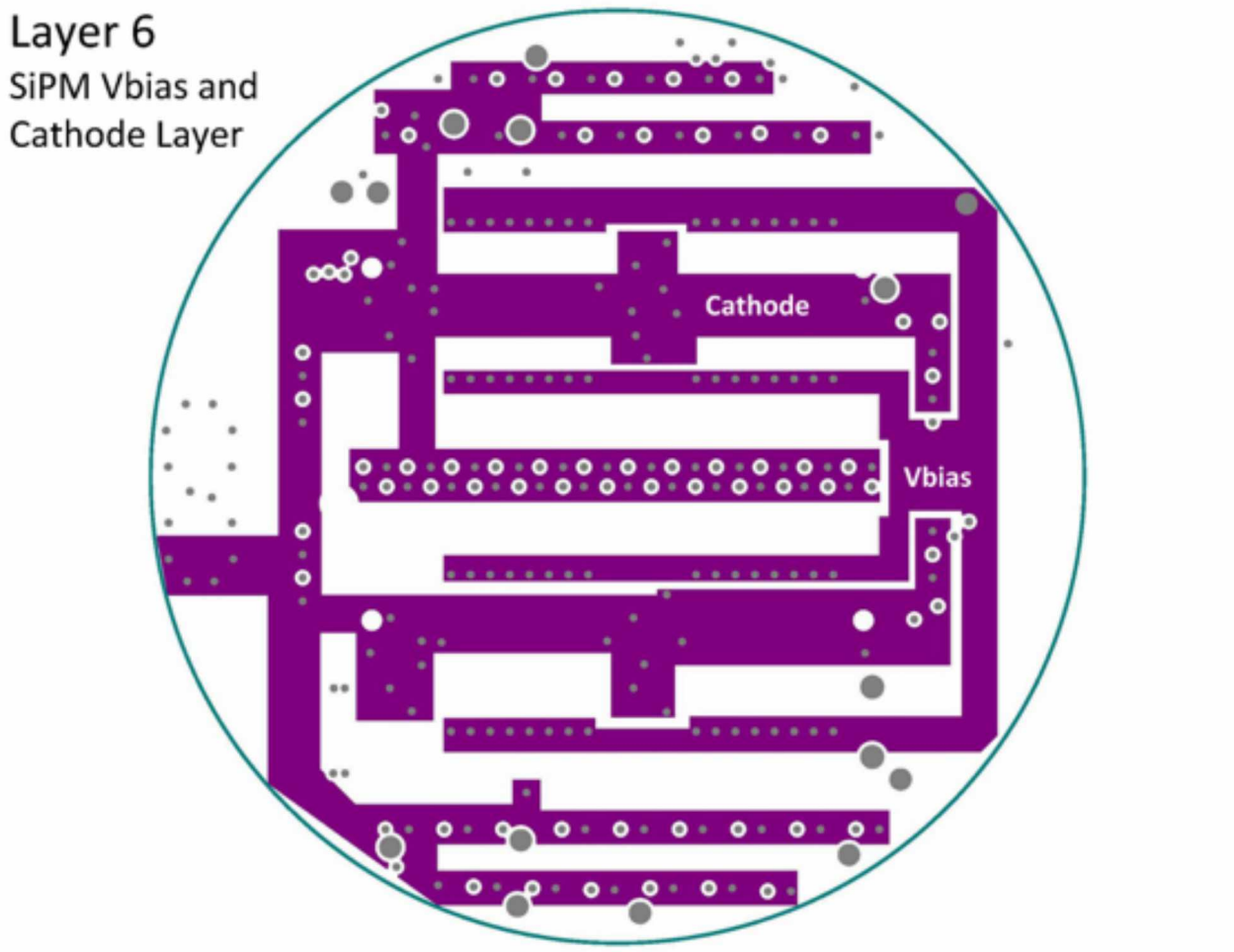
Layer 6
SiPM Vbias and
Cathode Layer
Cathode
Vbias

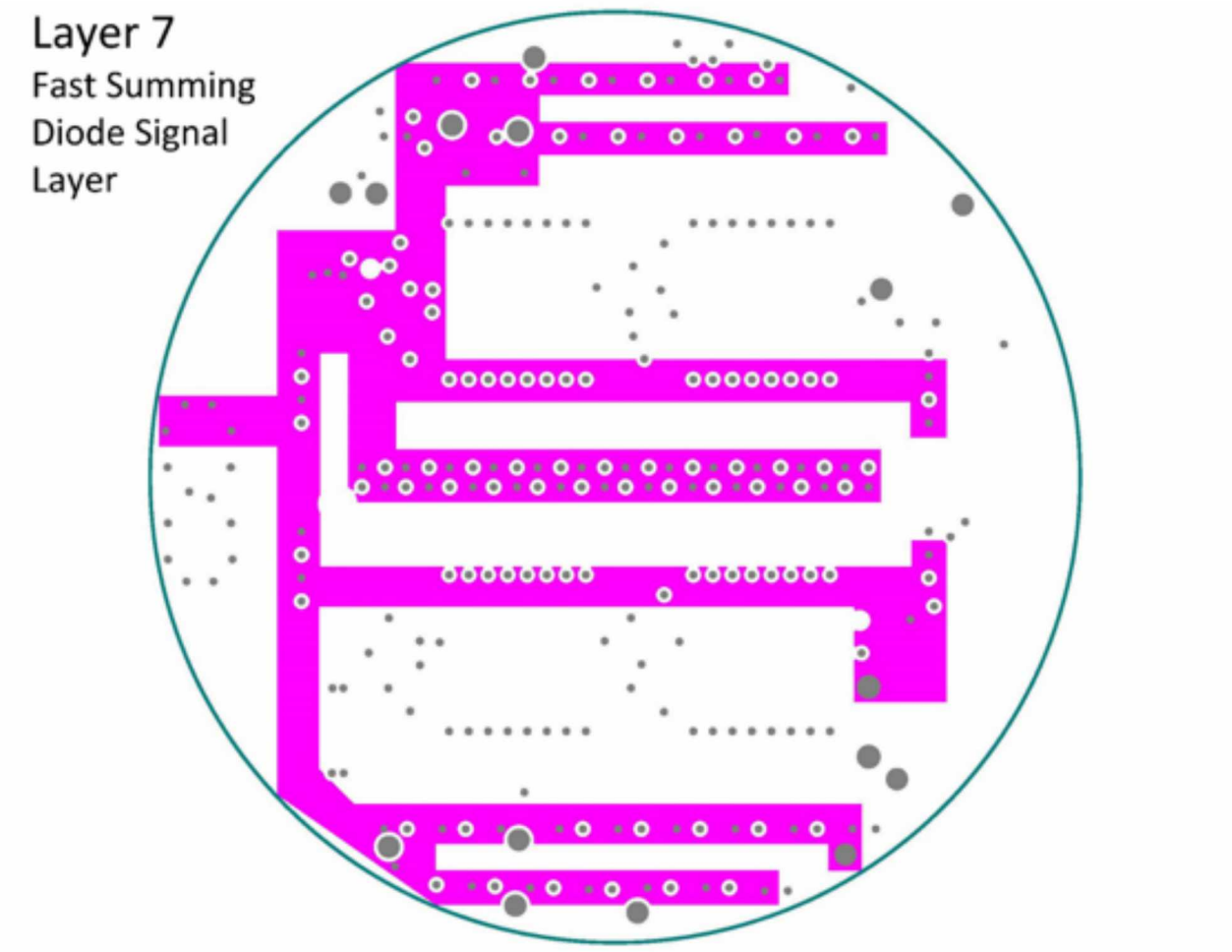
Layer 7
Fast Summing
Diode Signal
Layer

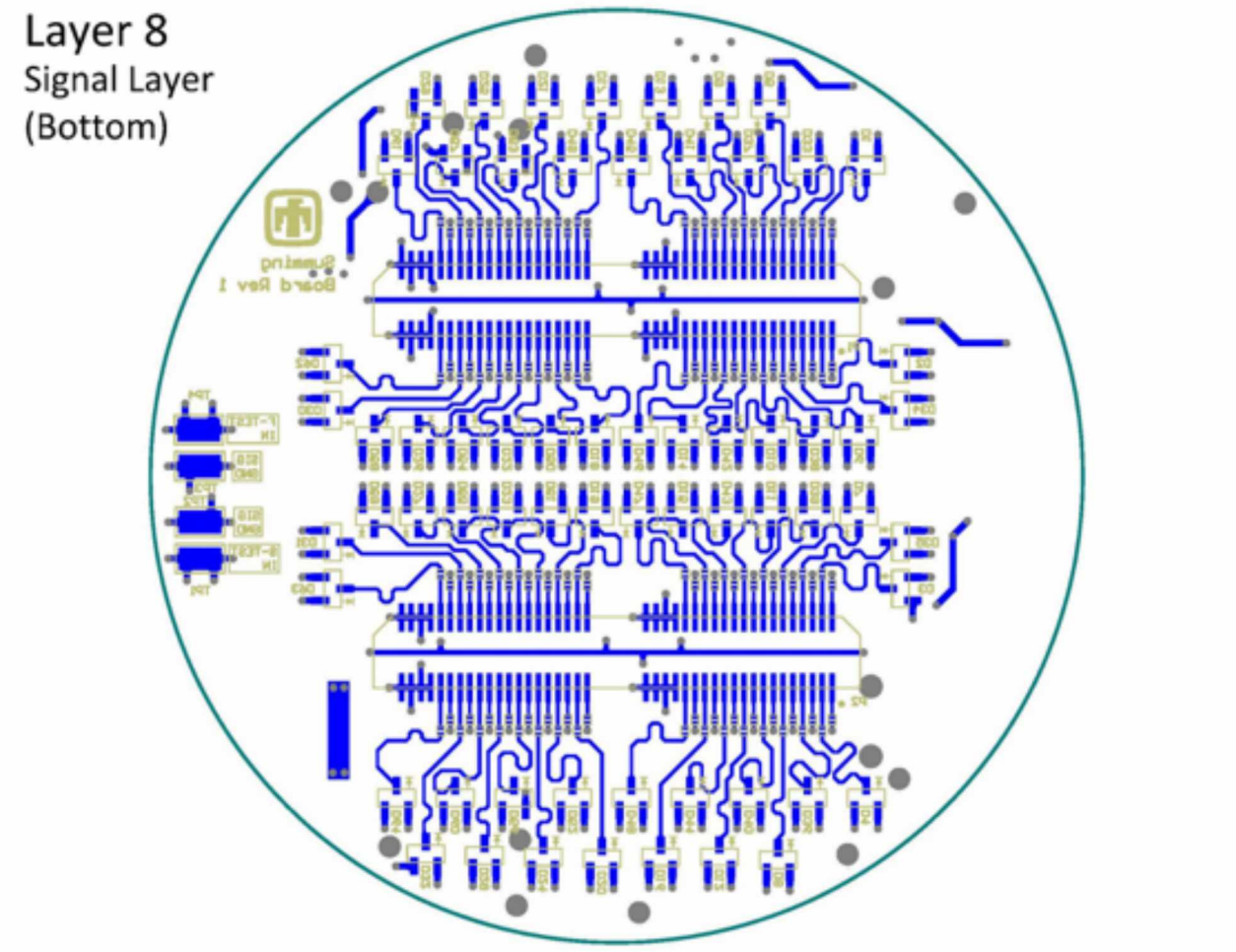
Layer 8
Signal Layer
(Bottom)

References

[1] M.Grodzicka-Kobylka, T.Szczesniak, M.Moszyski, L.Swiderski, D.Wolski, J.Baszak, S.Korolczuk, P.Schotanus. *Nucl. Inst. and Meth. in Phys. Res. A* **883** (2018) 158-165

[2] M. L. Ruch, M. Flaska, S. A. Pozzi *Nucl. Inst. and Meth. in Phys. Res. A* **793** (2015) 1-5

[3] J. Yu, Z. Wei, M. Fang, Z. Zhang, C. Cheng, Y. Wang, H. Su, Y. Ran, Q. Zhu, H. Zhang, K. Duan, M. Chen, M. Liu *Nucl. Inst. and Meth. in Phys. Res. A* **894** (2018) 129-137

[4] M. L. Ruch, M. Flaska, S. A. Pozzi *Nucl. Inst. and Meth. in Phys. Res. A* **793** (2015) 1-5

[5] Photomultiplier Tubes, Basics and Applications, Third Edition *Hamamatsu Photonics* (2007) www.hamamatsu.com/resources/pdf/etd/PMT_handbook_v3aE.pdf, Accessed on May 3rd, 2017.

[6] G. Romeo, G. Bonanno, S. Garozzo, A. Grillo, D. Marano, M. Munari, M.C. Timpanaro, O. Catalano, S. Giarrusso, D. Impiombato, G. La Rosa, G. Sottile *Nucl. Inst. and Meth. in Phys. Res. A* **826** (2016) 31-38

[7] R. Brun and F. Rademakers. *Nucl. Inst. and Meth. in Phys. Res. A* **389** (1997) 81-86

[8] J.E.M. Goldsmith, M.D. Gerling and J. S. Brennan *Review of Scientific Instruments* **87** (2016) 083307

[9] SensL, "C-Series Low Noise, Fast, Blue-Sensitive Silicon Photomultipliers, User Manual" Rev. 1.6, October 2015

[10] SensL, "ArrayC PCB Arrays of SiPM User Manual" Rev. 3.2, March 2017

[11] SensL"C-Series Low Noise, Fast, Blue-Sensitive Silicon Photomultipliers, Datasheet", Rev. 2.0, November 2015

[12] Mini-Circuits, "Evaluation Board and Circuit" DWG NO: TB-414-6A-20+, Rev. A, Sheet 3 of 3.

[13] SensL "Readout Methods for Arrays of SiPM, Application Note", Rev. 2.0, March 2015

[14] Texas Instrument, "DCR01 Series, 1-W, 1000-Vrms Isolated, Regulated DC-DC Converter Modules", Datasheet, SBVS013D-October 2001-Revised June 2016.

DISTRIBUTION:

1	MS 0899	Technical Library, 8944 (electronic copy)
1	MS 0359	D. Chavez, LDRD Office, 1911

Sandia National Laboratories